Construction of PWR nuclear cross sections for transient calculations. Test of the ANTI program against TWODIM

Forskningscenter Risø, Roskilde

Publication date:
1981

Document Version
Publisher's PDF, also known as Version of record

RISØ-M-2264

CONSTRUCTION OF PWR NUCLEAR CROSS SECTIONS FOR TRANSIENT CALCULATIONS. TEST OF THE ANTI PROGRAM AGAINST TWODIM

Bjørn Thorlaksen

Abstract. Nuclear cross sections for fuel assemblies of the more recent Westinghouse designs, representing two different PWR reactor cores, are calculated as functions of average fuel temperature, moderator density, and moderator poison concentration. The cross-section functions are verified by referring to Westinghouse power-shape calculations and other analyses.

Computations on the side reflector resulted in significantly higher albedo values than used previously for BWR's in similar nodal codes. This led to an investigation of the influence of the internodal coupling coefficients on the power shape. It is concluded that the calculated power shape is strongly dependent, on the choice of coupling coefficients. However, it is shown that "the correct" set of coupling coefficients depends mostly on the nodal configuration, and that it is fairly independent of the power condition.

INIS descriptors: COMPUTER CALCULATIONS; COUPLING CONSTANTS; CROSS SECTIONS; POWER DISTRIBUTION; PWR TYPE REACTORS; TRANSIENTS

May 1981
Risø National Laboratory, DK 4000 Roskilde, Denmark

UDC 621.039.51 : 621.039.524.4-98 : 681.3.06

ISBN 87-550-0768-6
ISSN 0418-6435

Risø repro 1981

CONTENTS

1. INTRODUCTION

In order to verify the 3-dimensional transient program ANTI (A.M. Larsen, 1980 and A.M. Larsen, E.F. Nielsen, 1980), a set of nuclear cross sections for a pressurized-water reactor was required. The present report describes the construction of such a data set and the verification of the cross sections against Westinghouse calculations. The verifications of the ANTI program against Westinghouse calculations and against calculations with the 2-dimensional finite difference program TWODIM (K.E. Lindstrøm Jensen, 1970 and G.K. Kristiansen, 1976) are also described.

Because data from an existing power plant was lacking a standardized 3000 MWt Westinghouse reactor was selected as reference. Most information about the reactor originates from the Westinghouse Reference Safety Analysis Report, RESAR 31.

The cross sections have been generated with the CRSIQ program (A.M. Larsen, 1973 and B. Lauridsen, 1977) and the CDB4 program (K.E. Lindstrøm Jensen, 1970 and C.F. Højerup, 1972). The programs are included in the Risø Reactor Physics Code System which was tested previously against calculations on both boiling-water reactors (A.M. Larsen et al., 1972) and pressurized-water reactors (H. Neltrup and P.B. Suhr, 1973).

2. DESCRIPTION OF THE REACTOR

2.1. General Description

The Reference Safety Analysis Report, RESAR 31 (Westinghouse, 1976) describes the Westinghouse standardized 3000 MWt three-loop nuclear steam supply system for a PWR. The steam supply

system (Fig.1) consists of the reactor and three closed reactor coolant loops connected in parallel to the reactor vessel. Each loop contains a reactor coolant pump and a steam generator. The nuclear steam supply system also includes an electrically heated pressurizer and certain auxiliary systems.

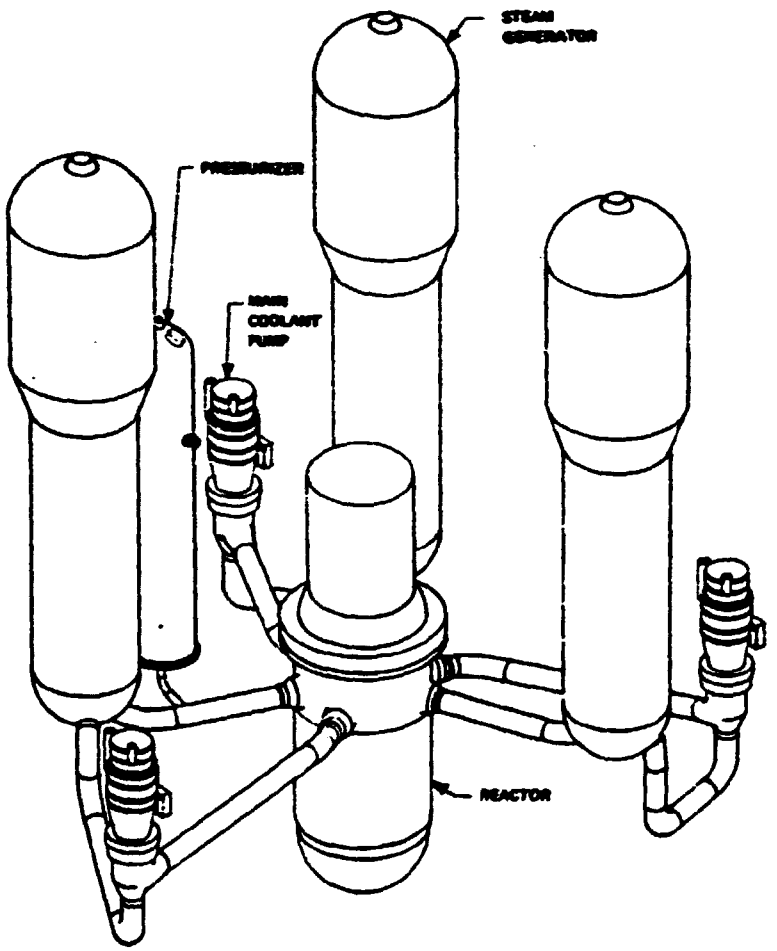

Fig. 1. Diagram of a three-loop nuclear steam supply system.

The 3000 MW_t plant is characterized by fuel with an active length of 4267 mm (168 in). Earlier Westinghouse plants had active fuel of 3658 mm (144 in). In Appendix A a comparison is given of the principal design parameters for reference plants with the two different fuel designs.

The reactor power is controlled by temperature coefficients of reactivity, by control rod cluster motion, and by neutron poison in the coolant in form of boric acid. The control rod cluster motion is required for load-follow transients and for startup and shutdown. The boron in the coolant is added during cold shutdown, partially removed at startup, and adjusted in concentration during core lifetime to compensate for burnup and fission product poisoning.

Given below is a short description of the reactor internals and their function as guidance for the coolant flow inside the reactor vessel. The components of the reactor internals are divided into three parts consisting of the lower support structure (including the core barrel and the neutron shield pad assembly), the upper core support structure, and the in-core instrumentation support structure. The reactor internals support the core, direct the coolant flow, and provide gamma and neutron shielding. The coolant flows from the vessel inlet nozzles down the annulus between the core barrel and the vessel wall and then into a plenum at the bottom of the vessel. The flow then reverses and flows up through the lower core support which provides the desired inlet flow distribution to the core. After passing through the core, the coolant enters the region of the upper support structure and then flows radially to the core barrel outlet nozzles and directly through the vessel outlet nozzles. A small portion of the coolant flows between the baffle plates and the core barrel to provide additional cooling of the barrel.

2.2 The reactor core

Overall description

The reactor core is composed of an array of 157 fuel assemblies which are identical in mechanical design, but different in fuel enrichment (Fig.2). Within an assembly the enrichment distribution of the fuel pins is uniform. The core is cooled and moderated by light water at a pressure of 155 bar. The concentration of the boron in the coolant is varied as required to control relatively slow reactivity changes including the effects of fuel burnup.

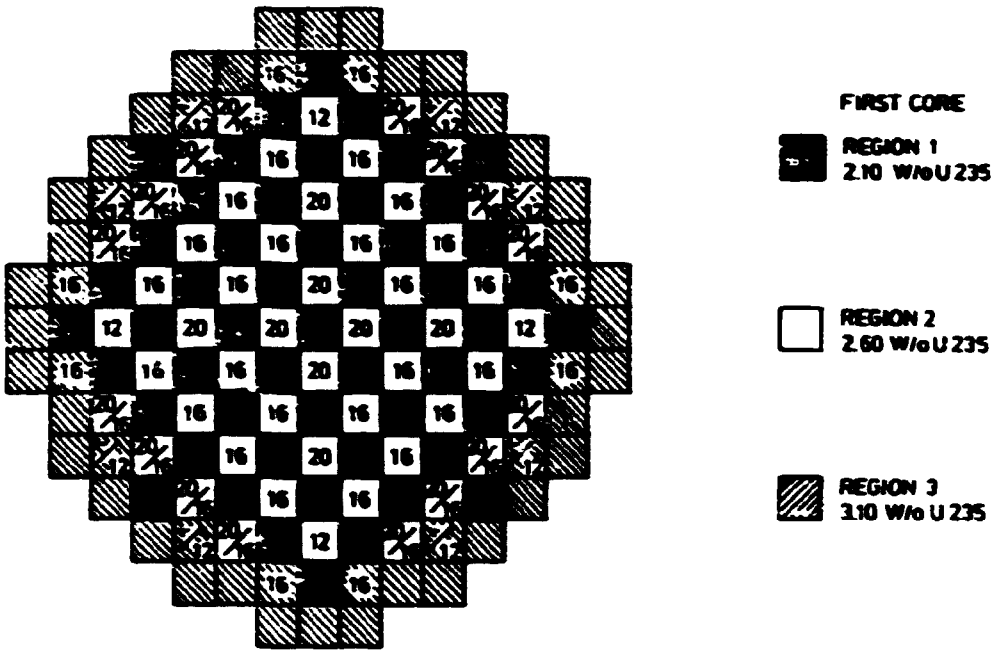

Fig. 2. Fuel assembly arrangement for RESAR 31 and Beaver Valley 1. The distribution of burnable poison rods in the first core is indicated by the number of rods per assembly. The boron rod distribution is slightly different for the two cores; if two numbers are indicated, the upper one refers to RESAR 31 and the lower one to Beaver Valley.

Additional boron, in the form of burnable poison rods, is employed in the first core to establish the desired initial reactivity. The distribution of boron rods for the recent core design, RESAR 31, is slightly different from the previous design, Beaver Valley. Both core designs are shown in Fig. 2.

The most effective control components are the full- and partial-length rod cluster control assemblies. The full-length rod cluster control assemblies provide reactivity control for shutdown, reactivity changes due to coolant temperature variations in the power range, reactivity changes associated with the power coefficient of reactivity, and reactivity changes due to void formation. The function of the partial-length rods is to control the axial power distribution during xenon transients and to limit axial xenon oscillations should they occur. In steady-state operation at constant power, insertion of the partial-length rods is not required. The rod cluster control assembly pattern is shown in Fig. 3.

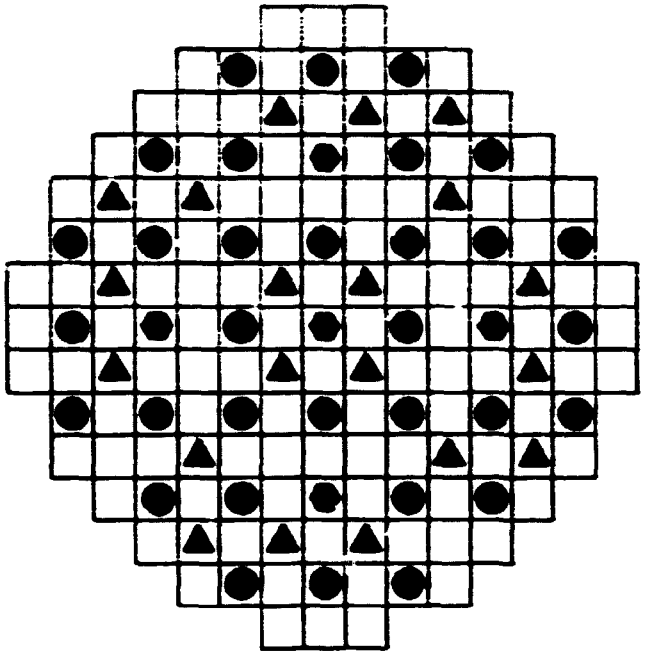

SIGNATURE		NUMBER OF CLUSTERS
●	CONTROL BANK A,B,C, and D	8 in each bank
▲	SHUTDOWN BANK S_A and S_B	8 " "
▲	" " S_C	4 " "
●	PART LENGTH P	5 " "

Fig. 3. Rod cluster control assembly pattern.

The fuel assembly

The 264 fuel rods in a fuel assembly are mechanically joined in in a 17 x 17 square array (Fig.4). The fuel rods are supported at intervals along their length by grid assemblies, which maintain the lateral spacing between the rods. The center position in the assembly is reserved for in-core instrumentation, while the remaining 24 positions in the array are equipped with guide thimbles joined to the grids and the top and bottom nozzles. Depending upon the position of the assembly in the core (Figs. 2 and 3) the guide thimbles are used as core locations for rod cluster control assemblies, neutron source assemblies, and burnable poison rods. Otherwise, the guide thimbles are fitted with plugging devices to limit bypass flow.

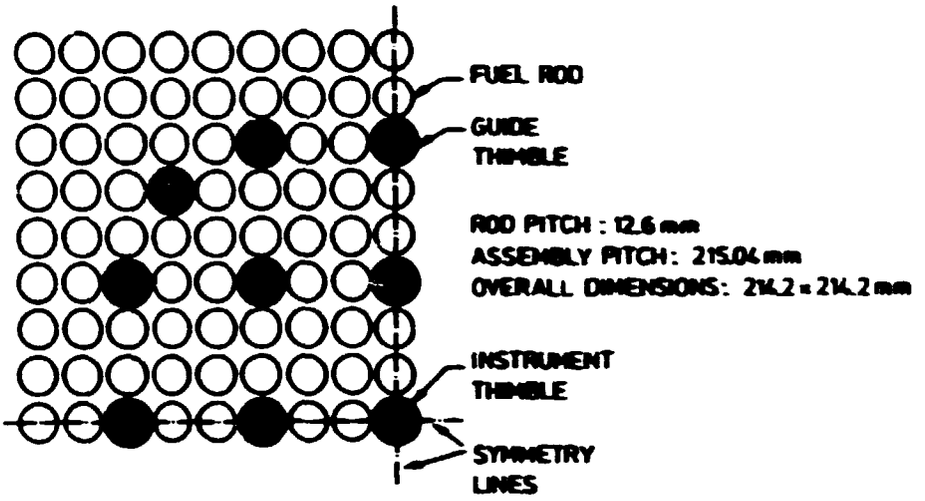

Fig. 4. Fuel assembly cross section. One-fourth of assembly.

Fuel rods

The fuel rods consists of slightly enriched UO_2 ceramic cylindrical pellets contained in zircaloy 4 tubings. The tubes are plugged and seal welded at the ends to encapsulate the fuel. All rods are pressurized with helium during the fabrication. The cross section of a fuel rod is shown in Fig. 5.

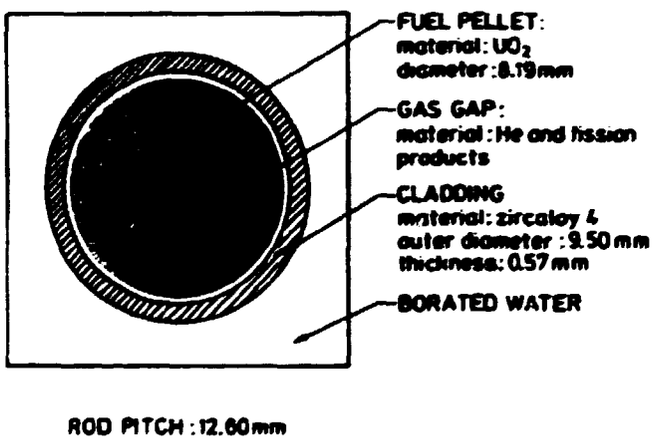

Fig. 5. Fuel rod cross section.

Guide thimbles

The guide thimbles are structural members which also provide channels for the neutron absorber rods, burnable poison rods, or neutron source assemblies. The thimble is fabricated from zircaloy 4 tubing having two different diameters. The large diameter at the top provides a relatively large annular area to permit rapid insertion of the control rods during a reactor trip as well as to accommodate the flow of coolant during normal operation. The lower portion has two sections with reduced diameter to produce a dashpot action near the end of the control rod travel.

Control assemblies

Each of the cluster control assemblies consists of a group of individual absorber rods fastened at the top to a common spider assembly. These assemblies are of two types, those with rods containing full length absorber material to control the reactivity of the core under operating conditions, and those with rods containing a partial-length absorber section (1067 mm) for control of the axial power distribution. The cross section of an absorber rod is shown in Fig. 6. The drives for the full-length rods are designed such that upon a loss of power to the magnetic coils, the rod cluster assembly is released and falls by gravity to shut down the reactor. Loss of power to the drives of the partial length rods will not result in any partial-length rod motion.

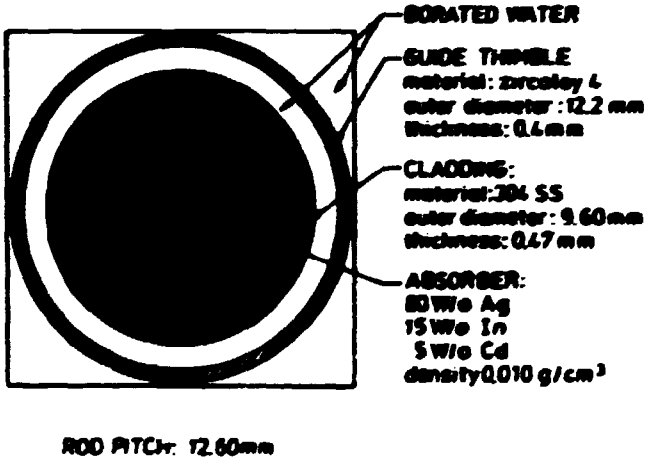

Fig. 6. Control rod and guide thimble cross section.

Burnable poison rods

The poison rods consist of borosilicate glass tubes contained within type 304 stainless steel tubular cladding which is plugged and seal welded at the ends to encapsulate the glass. The glass is also supported along the length of its inside diameter by a thin-walled turbular inner liner. The top end of the liner is open to permit the diffused helium to pass into the void volume, and the liner overhangs the glass. The liner has an outward flange at the bottom end to maintain the position of the liner with the glass. The cross section of a burnable poison rod is shown in Fig. 7. The rods are positioned in selected guide thimbles within the fuel assemblies and a fuel assembly can have either 12, 16, 20, or no burnable poison rods (Figs. 2 and 8).

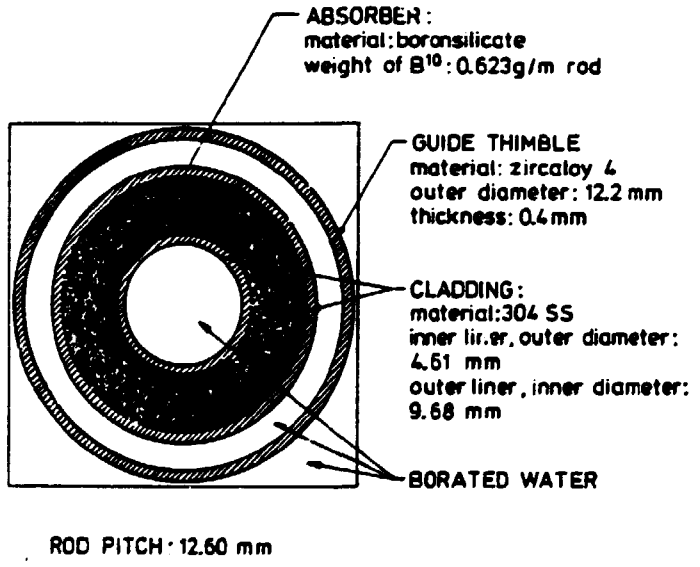

Fig. 7. Cross section of a burnable poison rod.

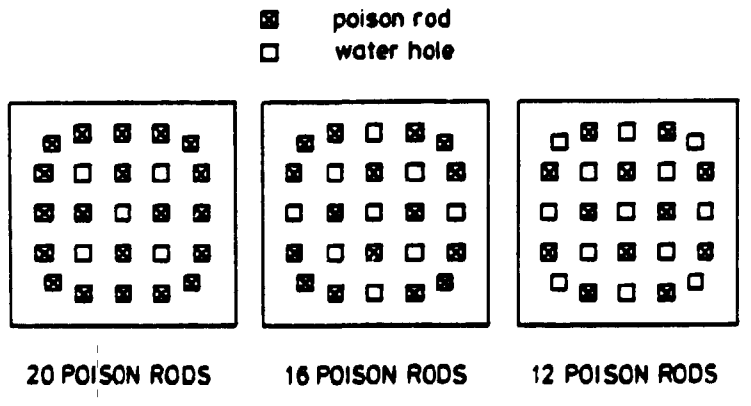

Fig. 8. Distribution of burnable poison rods within an assembly. The fuel assembly arrangement is given in Fig. 2.

2.3. The reflector

The active core is surrounded by borated water and stainless steel. The top and bottom reflectors have each a thickness of approximately 25 cm, and the side reflector is 38 cm thick. Detailed information about the composition of the axial reflectors was not found in RESAR 31, so the description below is devoted to only the radial reflector.

The lower core support structure is the main part of the side reflector. This support structure assembly consists of the core barrel, core baffle, neutron shield pads, and core support which is welded to the core barrel, Fig. 9.

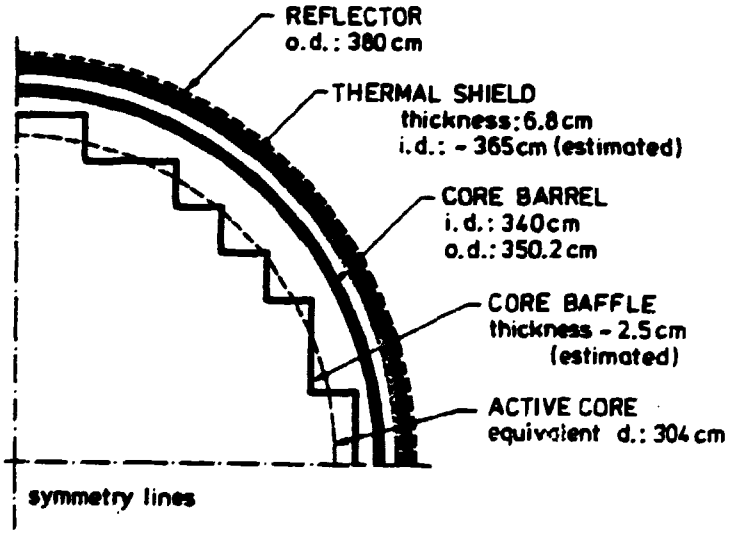

Fig. 9. Cross section of the side reflector. One-fourth of core.

All the major material for this structure is type 304 stainless steel. The core baffle is attached to the core barrel inner wall and forms the enclosure periphery of the assembled core.

The lower core support structure and the core barrel serve to provide passageways and control for the coolant flow. The neutron shield pad assembly consists of four pads that are bolted and pinned to the outside of the core barrel.

3. MODIFIED REACTOR CORE AND REFLECTOR DESIGN

For calculations of the nuclear cross sections it was necessary to use a slightly modified reactor design. A description of the geometry of the modified model is given in this chapter and the material number densities of the different regions are listed in Appendix B.

3.1 Pin cells

The fuel pin cell

For the fuel pin calculations an equivalent cell of three cylindrical regions was used (Fig.10). The area of the moderator region is the same as in the real square lattice.

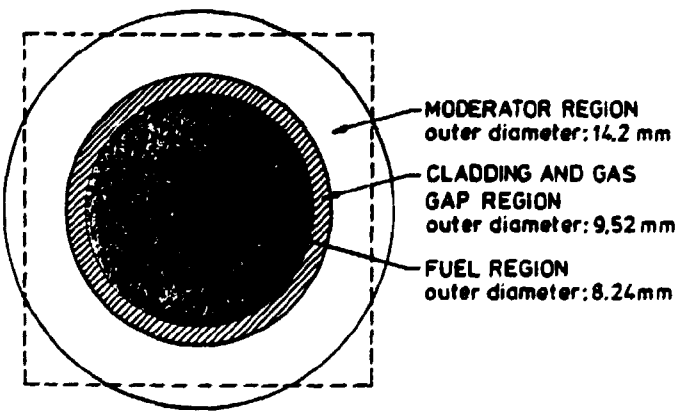

Fig. 10. Fuel rod equivalent cell.

The gas gap and the cladding are homogenized and the amount of spacer material corresponding to the pin cell is included in the cladding region. The influence of fuel and cladding temperature variations on the cell geometry and material densities is neglected. The equivalent cell corresponds to an average fuel temperature of 675 ^{o}C and an average cladding temperature of 350 ^{o}C.

Guide thimble cells

For the water pin, boron pin, and control pin cells it is necessary to include a driver zone as neutron source in the calculations. The driver zone is composed of the eight neighbouring fuel pin cells adjacent to the guide thimble cell (Fig.11).

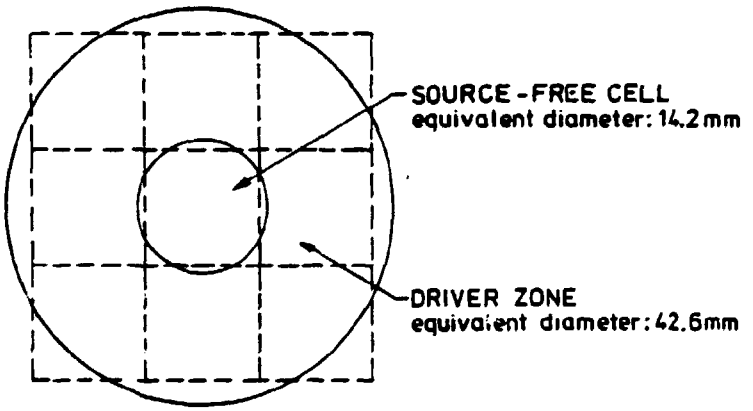

Fig. 11. Driver zone for guide thimble cells.

The equivalent cells for the water-, control-, and boron pins are shown in Figs. 12-14, respectively. The amount of spacer material corresponding to each cell is included in the guide thimble region. The moderator density of the inner moderator

region is kept constant (no void) even in case changes occur in the outer moderator density. The boron concentration (ppm) in the coolant is the same for the inner and outer moderator.

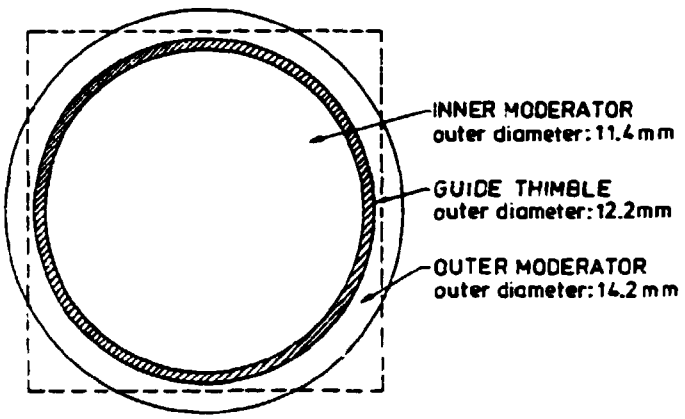

Fig. 12. Water pin equivalent cell.

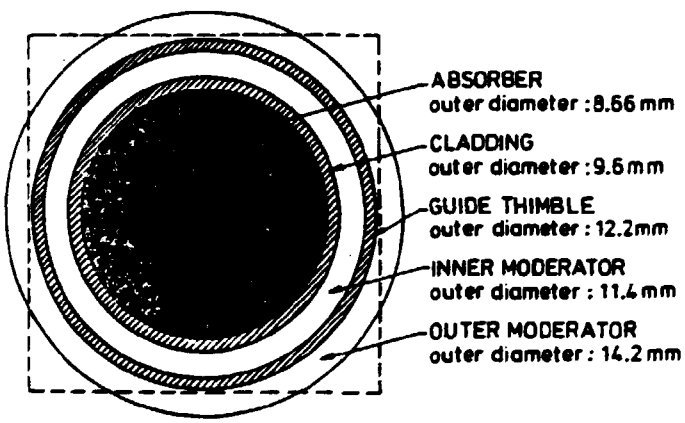

Fig. 13. Control pin equivalent cell.

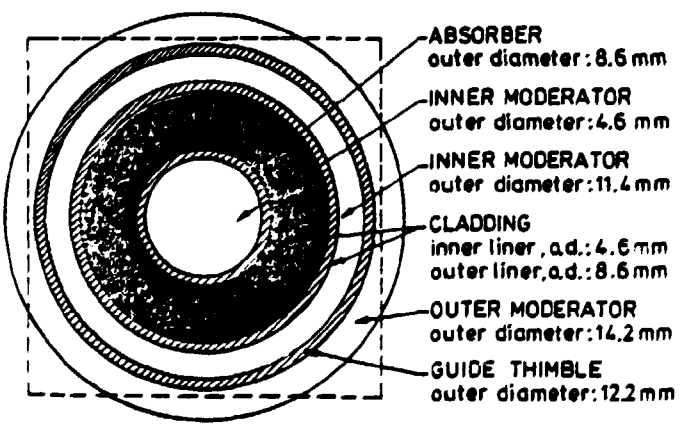

Fig. 14. Boron pin equivalent cell.

3.2. Fuel assemblies

The equivalent fuel assembly is composed of 264 identical fuel pin cells and 25 source-free pin cells arranged in a 17 x 17 array. The pin cell array is surrounded by a narrow watergap of 0.43 mm width so the assembly cell overall dimension becomes 215.06 x 215.06 mm^2.

For the two core configurations, RESAR 31 and Beaver Valley 1, a total of 9 different fuel assemblies are needed (Fig.2). The assemblies differ in fuel pellet enrichment, number of boron rods per assembly, and whether a control assembly is present or not. The characteristics of the nine assemblies are listed in Table 1. For each assembly the nuclear cross sections must be calculated as functions of moderator density, fuel temperature, and concentration of boron in the moderator.

Fuel assembly No.	Enrichment Wt % U235	Number of boron rods	+ with control rod - without control rod
1	2.10	0	-
2	2.10	0	+
3	2.60	12	-
4	2.60	16	-
5	2.60	20	-
6	3.10	0	-
7	3.10	0	+
8	3.10	16	-
9	3.10	12	-

Table 1. Fuel assembly characteristics.

3.3. Reflectors

So far no attempt has been made to calculate albedo values for the top and the bottom reflectors. For the side reflector first 2-group gamma-matrices are generated; these are then transformed to albedos (Chapter 4).

For calculating the 2-group cross sections for the side reflector materials the cylindrical geometry in Fig. 15 was used. Compared with Fig. 9 the core baffle ought to be closer to the core and the core barrel and the thermal shield should be separated with a watergap. An accurate description of the actual geometry of the side reflector was not found in RESAR-31. However, Fig. 9 is expected to be more correct. Whether or not the core barrel and thermal shield are kept close to each other is not believed to alter the results significantly, but an incorrect core baffle position might have some influence on the results.

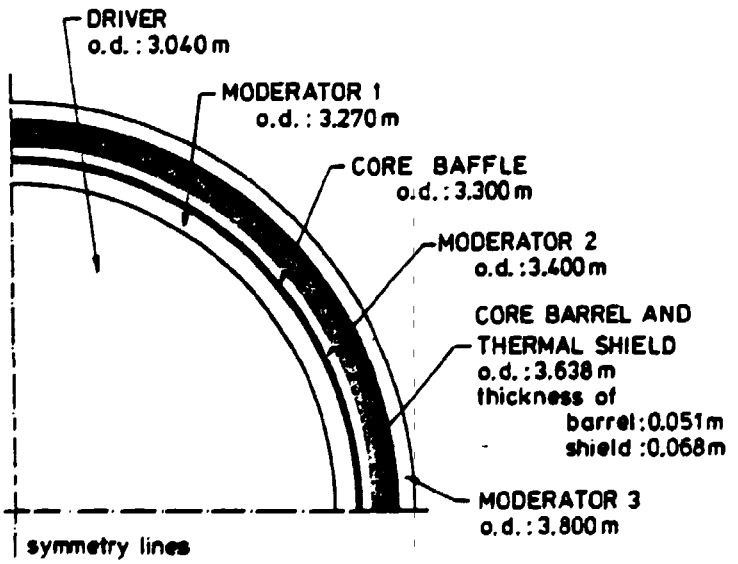

Fig. 15. Equivalent reflector geometry for calculating cross sections for the side reflector regions.

The reflector is represented either by gamma matrices or albedos. It is possible to convert a gamma matrix to an albedo (cp. 4.2). By means of the 2-group cross sections for the individual reflector regions, gamma matrices for the reflector are calculated in slab geometry. Two matrices are calculated, representing either the conditions close to the quarter-axis or an average condition (Fig.16). In both cases the core baffle position was close to the active core.

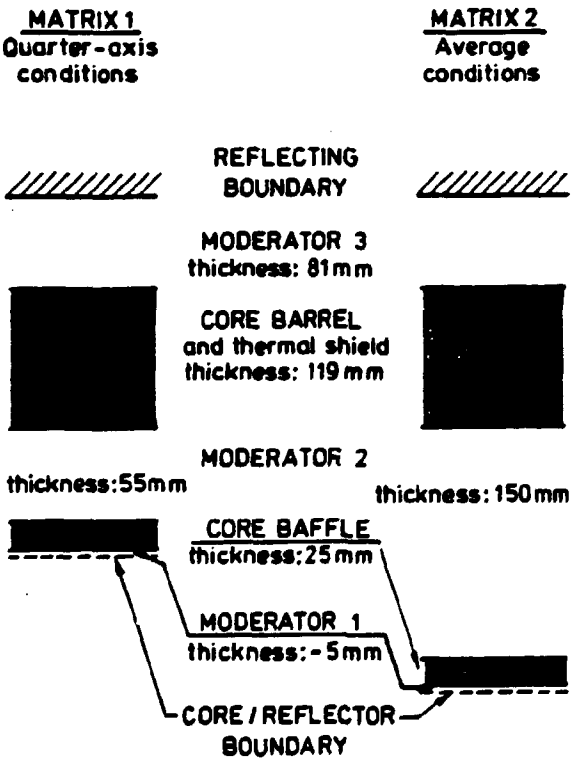

Fig. 16. Slab geometry for calculating gamma matrices for the side reflector.

4. CONSTRUCTION OF CROSS SECTIONS

4.1. Computer codes

For each of the nine different fuel assemblies in the reactor core 2-group cross sections are required as functions of the parameters: fuel temperature, moderator density, and boron concentration. The fuel box code CDB (K.E. Lindstrøm Jensen, 1970) may handle fuel pins of different compositions and non-burnable regions, e.g. water holes and control rods, burnable poison in the fuel, and burnable poison rods. The program combines the unit cell flux distribution and burnup calculations with a 2-dimensional diffusion theory flux solution for the fuel assembly, yielding power distributions, isotopic concentrations, box average cross sections, etc. as functions of the burnup. The number of energy groups for the pin cell and assembly flux calculations is flexible; however, 10 and 5 groups are recommended, respectively. The pin cell flux calculation may be omitted for pin cells without burnable material. If so, the pin cell should be represented by 5-group single-region macroscopic cross sections for the assembly flux calculation; otherwise 10-group multiregion microscopic cross sections are required.

The multigroup cross sections required by CDB for the pin cells are provided with the program complex CRS (A.M. Larsen, 1973). CRS gets fine group data from the SIGMA Master Tape and RESAB or RESOREX and supplements with thermal scattering matrices from the subroutine NELKINSCM. The subroutine GP calculates the fine group spectrum using multiregion probability methods in a specified cylinder cell. The number of fine groups is 76.

The radial reflector is represented by 2-group gamma matrices, which are produced by HECS (J. Pedersen, 1969) using collision probability methods. The gamma matrix is defined from the matrix equation

$$\underline{J} = \underline{\underline{\gamma}}\ \underline{\Phi} \qquad (4.1.1)$$

where $\underline{J}$ and $\underline{\emptyset}$ represents the boundary neutron current and flux, respectively. The 2-group multiregion macroscopic cross sections required for the HECS calculation are generated by CRS.

4.2. Reflector representations

One of the purposes of the present work was to test the static neutronics part of the 3-dimensional transient program ANTI (A.M. Larsen, 1980). ANTI is a nodal program and it utilizes a 1-group albedo representation for the reflector boundary. For verification of ANTI the 2-dimensional finite difference program TWODIM (K.E. Lindstrøm Jensen, 1970) was used. The reflector representation in TWODIM is a 2-group gamma-matrix representation; hence for comparing ANTI and TWODIM a transformation of gamma-matrices to albedos is required. Such a transformation of a 2-group gamma-matrix to a 1-group albedo is given below.

According to diffusion theory, the neutron currents in the positive and negative directions are, respectively,

$$J_+ = \frac{\emptyset}{4} + \frac{J}{2}$$

$$J_- = \frac{\emptyset}{4} - \frac{J}{2} \qquad (4.2.1)$$

The net neutron current is $J = J_+ - J_-$ and $\emptyset$ is the neutron flux. The albedo, β, is defined as

$$\beta = \frac{J_-}{J_+} = \frac{\frac{1}{2}-\gamma}{\frac{1}{2}+\gamma} \text{ , and } \gamma = \frac{J}{\emptyset} \qquad (4.2.2)$$

The superposition principle is applied for fluxes and currents in group theory, so the 2-group expressions for the net flux and the net current are as follows

$$\emptyset = \emptyset_1 + \emptyset_2$$

$$J = J_1 + J_2 \qquad (4.2.3)$$

The 2-group gamma-matrix is defined by

$$\begin{bmatrix} J_1 \\ J_2 \end{bmatrix} = \begin{bmatrix} \gamma_{11} & 0 \\ \gamma_{12} & \gamma_{22} \end{bmatrix} \begin{bmatrix} \phi_1 \\ \phi_2 \end{bmatrix} \qquad (4.2.4)$$

Using Eqs. 4.2.3 and 4.2.4 the final expression for the 1-group albedo (Eq. 4.2.2) is

$$\beta = \frac{\frac{1}{2}-\gamma}{\frac{1}{2}+\gamma} \text{ , and } \gamma = \frac{\gamma_{11}+\gamma_{12}+\gamma_{22}\,\frac{\phi_2}{\phi_1}}{1+\frac{\phi_2}{\phi_1}} \qquad (4.2.5)$$

The flux ratio should represent the value at the boundary between the active core and the reflector.

4.3. Pin cell and assembly calculations

For each of the 9 fuel assemblies listed in Table 1 cross sections should be found as functions of the fuel temperature, the moderator density, and the boron concentration in the moderator. The cross section functions should cover normal operating conditions and operational transient conditions.

As reference condition we chose:

fuel temperature	:	675°C	
moderator density	:	705 kg/m^3	(4.3.1)
boron concentration	:	900 ppm	

Extending from the reference condition, the fuel temperature and the moderator density were varied within the range given in Fig. 17.

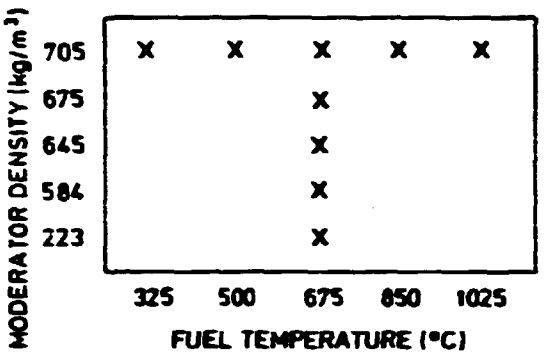

Fig. 17. Values of fuel temperature and moderator density for which fuel assembly calculations were carried out.

According to fuel pin cell studies the dependency of the boron concentration on the cross sections was extremely linear, so the assembly calculations in Fig. 17 were carried out for only two boron concentrations, namely 0 and 900 ppm. To attain high accuracy, cross sections should be calculated for each of the pin cells as functions of all the three parameters given above. However, pin cell calculations are rather time consuming, especially for the source-free pin cells where driver zones are required. Hence, for these cells, where the fuel temperature dependency is a secondary effect, moderator effects were predominantly considered.

The material number densities for the various cells are given in Appendix B, and the resulting cross sections for the assemblies are listed in Appendix C.

For use in ANTL, a polynomial representation of the assembly cross sections was found to be most adequate. By means of the non-linear least-squares fitting program CROSSFIT polynomia expressions were constructed. The expressions have the following form

$$D^1 = c_1 (1 + c_2R + c_3R^2)$$

$$D^2 = c_4 (1 + c_5R + c_6R^2 + c_7R^3) (1 + c_8B)$$

$$\Sigma_s^{12} = c_9 (1 + c_{10}R + c_{11}R^2 + c_{12}R^3) (1 + c_{13}T) (1 + c_{14}B)$$

$$\Sigma_a^1 = c_{15} (1 + c_{16}R + c_{17}R^2) (1 + c_{18}T) (1 + c_{19}B)$$

$$\Sigma_a^2 = c_{20} (1 + c_{21}R + c_{22}R^2) + c_{23}B (1 + c_{24}R)$$

$$\nu\Sigma_f^1 = c_{25} (1 + c_{26}R + c_{27}R^2)$$

$$\nu\Sigma_f^2 = c_{28} (1 + c_{29}R + c_{30}R^2) + c_{31}B (1 + c_{32}R)$$

$$\nu = c_{33}$$

(4.3.2)

The parameters are

D_1, D_2 Diffusion constants for the fast and thermal neutron group, respectively (cm)

Σ_s^{12} Down scattering cross section (cm^{-1})

Σ_a^1, Σ_a^2 Absorption cross sections, fast and thermal group, respectively (cm^{-1})

Σ_f^1, Σ_f^2 Fission cross sections, fast and thermal group, respectively (cm^{-1})

$\nu=\nu^1=\nu^2$ Number of neutrons produced per fission

ρ_m Moderator density (g/cm^3)

B_m Boron concentration in moderator (ppm)

T_f Fuel temperature (K)

$$R = \rho_m - \rho_{mo}$$

$$B = B_m - B_{mo}$$

$$T = \sqrt{T_f} - \sqrt{T_{fo}}$$

The subscript "o" refers to the reference condition.

For each fuel assembly two sets of coefficients, c_i, i=1,33, were calculated. The two sets represent new fuel either with Xe/Sm in equilibrium or without Xe/Sm. The polynomial coefficients are listed in Appendix D.

4.4. Reflector calculations

Calculations of reflector values were carried out only for the reference condition. The two gamma-matrices described in Chap. 3.3 obtained the following values

$$\text{Quarter-axis condition: } \begin{bmatrix} 0.1639 & 0 \\ -0.0454 & 0.1622 \end{bmatrix}$$

$$\text{Average condition} \quad : \begin{bmatrix} 0.1491 & 0 \\ -0.0345 & 0.1624 \end{bmatrix} \qquad (4.4.1)$$

To convert the gamma-matrices to albedos the 2-group flux ratio along the core boundary is required (Eq. 4.2.5). Using the gamma-matrices as boundary conditions the flux ratio along the periphery of the active core was found. The result of the calculations became an albedo of 0.60 with an insignificant variation along the core boundary (less than 0.01). The calculations were repeated for a reflector where the basic form of the core baffle was a cylinder, i.e. the core baffle was removed a small distance from the active core. These calculations resulted in almost the same albedo value.

5. OVERALL CALCULATIONS

5.1. Comparison of TWODIM calculations with Westinghouse results

A version of the TWODIM program was modified for handling the cross sections in a form similar to that of ANTIs. However, TWODIM needs a full 2-group scattering matrix and from the functions given in Eq.4.3.1. only the following matrix elements can be found:

$$\Sigma^{11} = \Sigma_a^1 + \Sigma_s^{12}$$

$$\Sigma_s^{12} \qquad (5.1.1)$$

$$\Sigma^{22} = \Sigma_a^2$$

For the missing parameters, i.e. Σ_s^{21}, ν^1, and the fission spectrum, the values corresponding to the reference condition were used.

TWODIM was applied for the calculation of the normalized horizontal power distribution for an unrodded Beaver Valley 1 core at hot full power. In this case the core baffle had the shape of a cylinder, the coolant inside the core baffle was represented by cross sections, and the remaining reflector was represented by gamma-matrices. Referred to Westinghouse results (Appendix E) the maximum error was 0.06. In the more realistic case with a core baffle following the core periphery, the result should improve a little, as the relative power at the reflector should then decrease slightly.

From the information given in the safety analysis reports, it was impossible by means of 2-dimensional calculations to verify the cross sections for the rodded fuel assemblies.

5.2. Comparison of ANTI and TWODIM calculations

The expression for the internodal coupling coefficients in ANTI involves the quantities:

r_h = the probability that a neutron leaving a node enters a neighbouring node in the same horizontal layer

r_v = the probability that a neutron leaving a node enters a neighbouring node in the same vertical channel

σ = the probability that a neutron will remain within the node where it is born

ρ = the probability that a neutron entering a node will be reflected directly to a neighbouring node

β = the probability that a neutron entering a node will be directly absorbed in that node

μ = the probability that a neutron entering a node can be treated as born in that node ($\rho+\beta+\mu=1$)

$\alpha = \frac{\beta}{\mu}$

In the program the probabilities are given as functions of the nodal dimensions, the local cross sections, and of 4 empirical parameters g_i, i=1 4. The expressions have the following form (Babala et al., 1971)

$$r_h = \frac{s^{g_1}}{2+4\ s^{g_1}} \qquad (5.2.1)$$

$$r_v = \frac{1}{2+4\ s^{g_1}} \qquad (5.2.2)$$

$$\sigma = 1 - \exp\ (-g_2\ a^2/\hat{M}) \qquad (5.2.3)$$

$$\alpha = g_3 \frac{a^2}{\bar{M}^2} \frac{\nu^2 \Sigma_f^2}{k} \tag{5.2.4}$$

$$\rho = \exp\ (- g_4 \sqrt{B^2}) \tag{5.2.5}$$

where

$s = \frac{\Delta X}{\Delta Z}$, ΔX and ΔZ are the horizontal and vertical dimensions of the node, respectively (5.2.6)

$$a = \frac{3\Delta X\ \Delta Z}{\Delta X + 2\Delta Z} \tag{5.2.7}$$

$$\hat{M} = \frac{\sqrt{D^1}}{\Sigma_a^1 + \Sigma_s^{12}} + \frac{\sqrt{D^2}}{\Sigma_a^2} \tag{5.2.8}$$

$$\bar{M}^2 = \frac{D^1}{\Sigma_a^1 + \Sigma_s^{12}} + \frac{D^2}{\Sigma_a^2} \tag{5.2.9}$$

k is the infinite multiplication factor for the node.

The ANTI calculations showed a very strong dependence on the choice of g-parameters. By means of more or less theoretical methods Babala et al., 1971 suggested the following g-set

$$\begin{aligned} g_1 &= 1.7 \\ g_2 &= 0.038 \\ g_3 &= 0.6 \\ g_4 &= 4.50 \end{aligned} \tag{5.2.10}$$

but in comparison with other codes g_3=3.07 appeared to be better, at least for BWR-systems. This g-set should be valid for nodal dimensions 10 cm $\leq \Delta X, \Delta Z \leq$ 20 cm and $0.5 \leq \Delta Z/\Delta X \leq 2$.

For the present work two different nodal configurations were studied. In both cases the nodes had an almost cubic shape with $\Delta X/\Delta Z = 1.008$, but with ΔX equal to either a 1/1 or 1/2 fuel pitch. For comparison with TWODIM two small 2-dimensional test-cases were studied. These included one horizontal layer of nodes

and 1/8 of the core periphery only. The axial albedos were both 1.0 corresponding to ideal reflecting conditions.

Compared with TWODIM calculations the g-set (5.2.10) did not fit the power distribution well; in the case of one node per fuel assembly, especially, the result was very poor. However, the reactivity was acceptable in both cases. If g_3=3.07, as suggested for BWRs, the power distribution became even worse. By varying g_3 it was found that the smaller is g_3, the better is the power distribution, but the reactivity decreases; even for g_3=0 the power distribution is unacceptable (Fig. 18).

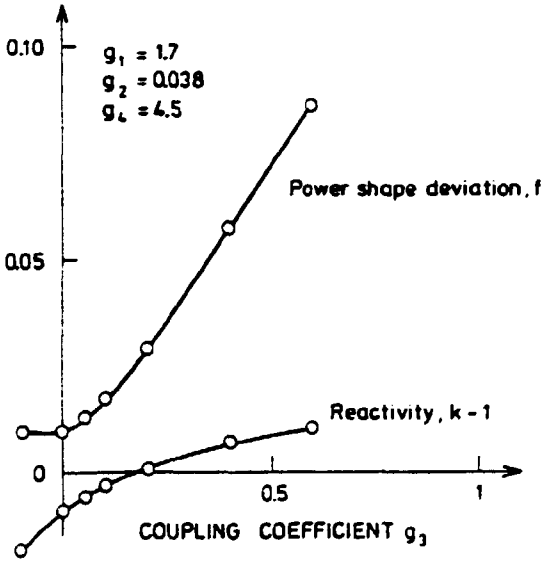

Fig. 18. Comparison of ANTI and TWODIM results for different values of g_3. In ANTI each fuel assembly is represented by one node. The power shape deviation is calculated as the square deviation of the horizontal power shapes normalized to one per node.

According to Fig. 19 a better power distribution can be established by changing g_4 instead of g_3, and in this case the reactivity is not altered so much. Finally, a variation of g_2 was

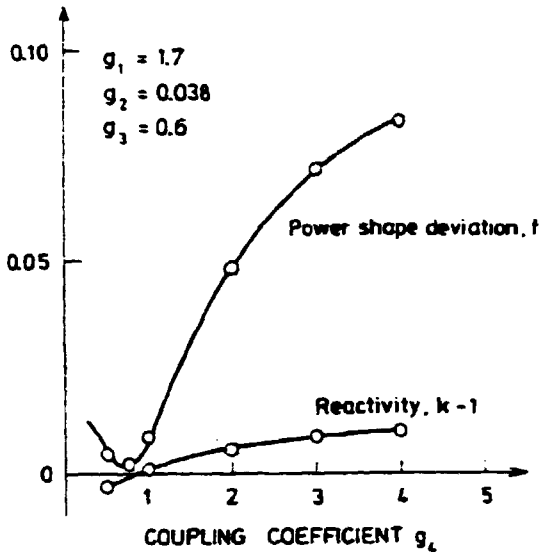

Fig. 19. Comparison of ANTI and TWODIM results for different values of g_4, and one node per assembly in ANTI. For the definition of the power shape deviation, f, see Fig. 18.

tried, but no further improvements of the results were obtained. Consequently, the following g-set was chosen for the case with one node per assembly

$$\begin{aligned} g_1 &= 1.7 \\ g_2 &= 0.038 \\ g_3 &= 0.6 \\ g_4 &= 0.65 \end{aligned} \qquad (5.2.11)$$

A similar method was applied in the case of 4 nodes per assembly. For this case the following g-set is suggested

$$\begin{aligned} g_1 &= 1.7 \\ g_2 &= 0.038 \\ g_3 &= 0.6 \\ g_4 &= 3.25 \end{aligned} \qquad (5.2.12)$$

There is no significant discrepancy in the accuracy of ANTI in the two cases with different nodal representations.

The investigations above were all performed at a hot operating condition with all control assemblies fully out of the core.

To investigate other power conditions, a few other power distributions were established by inserting control assemblies and increasing the reaction rate at local spots, but maintaining the g-sets. A significant discrepancy between TWODIM and ANTI was found only in the case of an extreme local power peak. In all other cases the accuracy was almost the same as in the reference case. The power distributions for the cases above are included in Appendix F.

As part of the Nordic reactor physics benchmark problem, 1980, a comparison of a 3-dimensional ANTI calculation and a 2-dimensional TWODIM calculation in cylindrical geometry was made (A.M. Larsen and B. Thorlaksen, 1980). In this case the nodal dimensions were DX=21.4 cm and DZ=25.0 cm and the coupling coefficients had the values given in Eq. 5.2.11. Even in this case there was good agreement between the power distributions calculated by ANTI and TWODIM.

According to the investigations above it can be concluded that the power shape calculated with the nodal method is extremely dependent on the choice of coupling coefficients. However, the "correct" g-factors are mostly dependent on the nodal configuration, and different operating conditions can be modelled fairly well with the same g-set.

5.3. Axial power distributions

As mentioned previously (p. 20) no attempt was made to estimate the efficiency of the top and bottom reflectors. These have no direct influence on the radial power distributions, and in fact the influence on the axial distribution is also modest.

Fig. 20 shows the axial power distribution for an unrodded reactor core of the Beaver Valley design. The calculation was made with the Swedish POLKA program, and is compared to a similar ANTI calculation. In the two cases the axial albedos were both 0.1. Although the neutronics of POLKA and ANTI is almost the

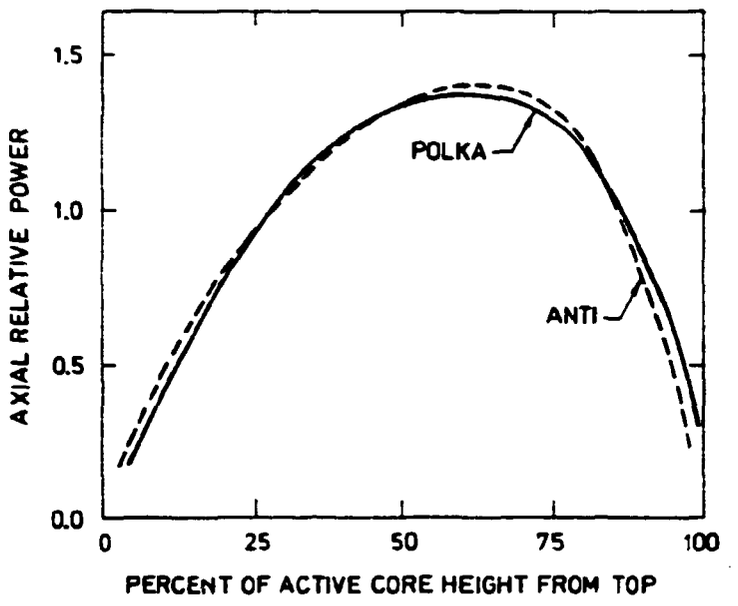

Fig. 20. Axial power shapes for an unrodded core calculated with ANTI and POLKA, respectively.

same, it is not obvious that the axial albedos should be equal, as the coupling coefficients are different. In fact, the radial albedoes in ANTI are about 50% larger than in the POLKA case. However, the deviation of the two curves in Fig. 20 is not significant, and by the fitting of either the coupling coefficients or the axial albedos, it should be possible to make the accordance even better. It seems as if the ANTI curve is slightly more peaked at the bottom end; this could also be due to different hydraulic models or moderator feed back systems.

In Fig. 21 an ANTI calculation is referred to the axial power distribution given by Westinghouse for a reactor state with the partlength control assemblies placed at the axial mid-plane. Obviously, the ANTI absorber is too strong compared to Westinghouse. In this case the ANTI power peak at the lower part of the core is more pronounced than in the previous case.

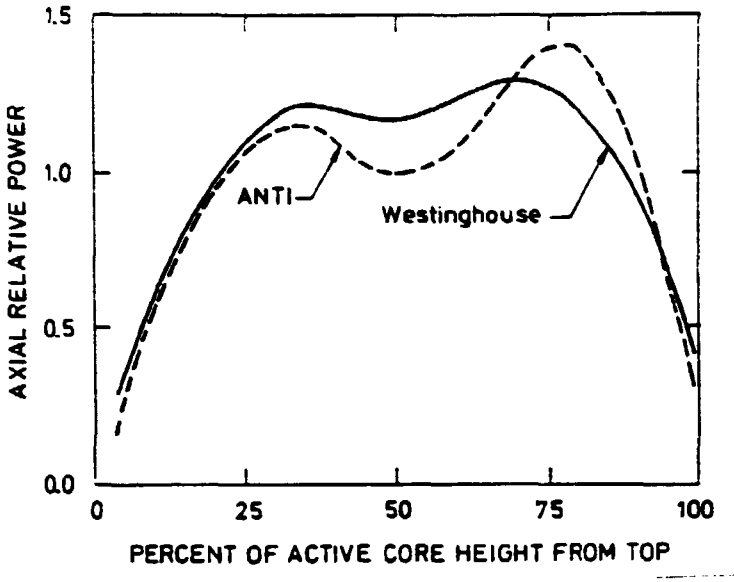

Fig. 21. Axial power shape calculated with ANTI and referred to Westinghouse for a core with the part-length control assemblies at the axial midplane. The deviation might be caused by differences in the active core height.

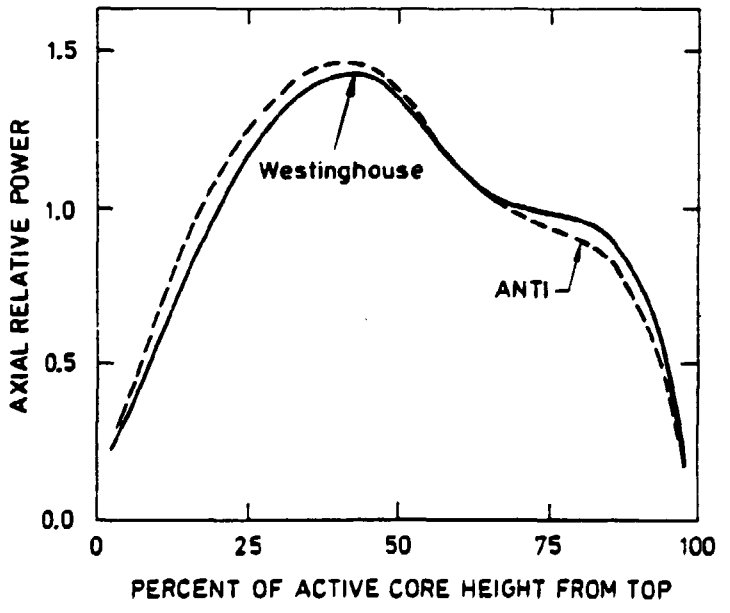

Fig. 22. Axial power shapes as in Fig. 21, but with the part-length control assemblies at the lower end of the core.

Fig. 22 represents a situation with the part-length assemblies at the bottom position, which, in this connection, means covering a region from about 55% to 80% from the core outlet. Even in this case the control power seems to be overestimated in ANTI, although the two curves almost merge.

According to the calculations above it is concluded that the coupling coefficients found previously from 2D-calculations can be used also for 3D-cases. Further, the top and bottom reflectors seem to have only a slight influence on the axial power distribution.

The neutron absorption of the ANTI control assemblies is strong compared to Westinghouse; however, the conditions are not specified in detail for the reference cases, so the value of the results cannot be fully estimated. The different degrees of control could be due to differences in the active core height. The ANTI calculations have been performed with an active core height of 4.26 m, which corresponds to the most recent core design. The Westinghouse results should also be valid for this design as they are included in RESAR 31; however, the curves seem to have been taken over from the final safety analysis report for Beaver Valley 1, which has an active fuel height of only 3.65 m. In both designs the part-length assemblies cover one quarter of the active fuel height.

6. CONCLUSION

Nuclear cross sections for nine different fuel assemblies of the more recent Westinghouse designs are calculated as functions of the average fuel temperature, moderator density, and moderator burnable poison concentration. For each assembly two data sets are given, each representing new fuel, but either

without Xe and Sm or with Xe and Sm in equilibrium concentrations.

The cross section functions were verified by referring to Westinghouse power shape calculations. From the nine fuel assemblies a reactor core of the most recent Westinghouse design, as described in RESAR 31, can be composed. Also earlier designs, as, for example, Ringhals 3 and Beaver Valley 1 can be represented.

Calculations on the side reflector resulted in significantly higher values of the reflector albedo referred to albedo values taken over from the ANDYCAP project. This led to an investigation of the influence of the ANTI internodal coupling coefficients on the power shape. It was concluded that the calculated power shape is strongly dependent, on the choice of coupling coefficients. However, it was shown that it is easy to find a set of coupling coefficients with which different operating conditions can be modelled quite well, if only the nodal configuration is unchanged.

REFERENCES

BABALA, D., BECH, N., HAUGSET, K (1971). ANDYCAP-Vol 1-Theory. SRD-40. Scandinavian Reactor Dynamic Project.

JENSEN, K.E. LINDSTRØM (1970). Development and Verification of Nuclear Calculation Methods for Light-Water Reactors. Risø Report No. 235. 161 pp.

KRISTIANSEN, G.K. (1976). The Finite-Difference Neutron Diffusion Programme TWODIM. Risø-M-1891. 19pp.

LARSEN, A.M. HVIDTFELDT (1980). The Three-Dimensional PWR Transient Code ANTI; Rod Ejection Test Calculation. RISØ-M-2209. 33pp.

LARSEN, A.M. HVIDTFELDT (1973). CRS: A Code to Produce Multigroup Neutron Cross Sections for Reactor Physics Calculations. RISØ-M-1568. 32pp.

LARSEN, A.M. HVIDTFELDT, LARSEN, H., PETERSEN, T. (1972). Calculations on a Boiling Water Reactor as a Test of the Risø Reactor Code Complex. Risø Report no. 268. 102 pp.

LARSEN, A.M., THORLAKSEN, B. (1980). Forslag til løsning af NRF BENCHMARK PROBLEM 1980: KONTROLSTAVSUDSKYDNING I EN BWR. DYN-3-80. Forsøgsanlæg Risø (in Danish).

LAURIDSEN, B. (1977). CRSIQ: A Cluster Programme to Produce Multigroup Cross Sections. RP-12-77. 17pp. Risø National Laboratory.

NELTRUP, H., SUHR, P.B. (1973). Survey of Calculations on the Haddam Neck (Connecticut Yankee) Power Plant as a Test of the Risø Reactor Physics Code System. Risø Report no. 298. 62 pp.

NIELSEN, E. FALCON, LARSEN, A.M. HVIDTFELDT (1980). Input Description for the Three-Dimensional PWR Transient Code ANTI. Risø-M-2256. 105 pp.

PETERSEN, J. (1969). Calculation of Heterogeneous Constants for Cylinders and Slabs. RISØ-M-850. 23 pp.

Reference Safety Analysis Report. RESAR 31, 3000 MWt NSSS (1976). Westinghouse Nuclear Europe,Inc.

APPENDIX A

The following tables compare the principal nuclear, thermo-hydraulic, and mechanical design parameters for two recent Westinghouse reference plants. The main difference between the two reactors is the height of the active core, which is either 4267 mm or 3658 mm. The Ringhals 3 and 4 reactors are of the latter design.

REACTOR DESIGN COMPARISON TABLES

THERMAL AND HYDRAULIC DESIGN PARAMETERS	RESAR-31 4267-mm Core (168 in)	Beaver Valley 3658-mm Core (12 ft)
Overall		
Reactor core heat output, MWt	2988	2652
Number of coolant loops	3	3
Heat generated in fuel, %	97.4	97.4
System pressure, nominal, bar	155	155
- - , min. steady state, bar	153	153
Coolant flow		
Total thermal flow rate, kg/s	$13.95 \cdot 10^3$	$12.71 \cdot 10^3$
Effective flow rate for heat transfer, kg/s	$13.3 \cdot 10^3$	$12.1 \cdot 10^3$
Effective flow area for heat transfer, m^2	3.86	3.86
Average velocity along fuel rods, m/s	4.98	4.4
Average mass velocity, $kg/(s \cdot m^2)$	3458	3146
Coolant temperature		
Nominal inlet, °C	293.4	283.6
Average rise in vessel, °C	36.5	37.4
Average rise in core, °C	38.0	39.0
Average in core ($\bar{H}$), °C	313.6	304.1
Average in vessel ($\bar{T}$), °C	311.6	302.3
Heat transfer		
Active heat transfer, surface area, m^2	5267	4515
Average heat flux, W/cm^2	55.29	57.2
Maximum heat flux for normal operation, W/cm^2	135.5	132.7
Average linear power, W/cm	165	170
Maximum linear power for normal operation, W/cm	404	394.4
Peak linear power for determing protection setpoints, W/cm	590.5	590.5
Heat flux hot channel factor, F_Q	2.45	2.45
Fuel central temperature		
Peak at 100% power, °C	1760	1816
Peak at peak linear power for determing protection setpoints, °C	2288	2288

CORE MECHANICAL DESIGN PARAMETERS	4267-mm Core (168 in)	3658-mm Core (12 ft)
Fuel assemblies		
Design	RCC canless	RCC canless
Number of fuel assemblies	157	157
UO_2 rods per assembly (17-17)	264	264
Rod pitch, mm	12.60	12.60
Overall dimensions, mm	214 × 214	214 × 214
Assembly pitch, mm	215.04	
Fuel weight (UO_2), kg	95863	82284
Zircaloy weight (total), kg	21953	18737
Number of grids per assembly	9-type B	8-type B
Composition of grids	Inconel 718	Inconel 718
Weight of grids (effective in core), kg	1090	855
Number of guide thimbles per assembly	24	24
Number of instrument thimbles	1(central)	1(central)
Composition of guide thimbles	Zircaloy-4	Zircaloy-4
Loading technique	3 region, non-uniform	3 region, non-uniform
Fuel rods		
Number	41448	41448
Outside diameter, mm	9.50	9.50
Diametral gap	0.17	0.17
Clad thickness, mm	0.57	0.57
Clad material	Zircaloy-4	Zircaloy-4
Fuel pellets		
Material	UO_2 sintred	UO_2 sintred
Density, % of theoretical	95	95
Diameter, mm	8.19	8.19
Length, mm	13.5	13.5
Mass of UO_2 per length of fuel rod, kg/m	0.542	0.542
Guide thimbles		
Diameter of guide thimbles (upper part), mm	i.d 11.4 o.d 12.2	i.d 11.4 o.d 12.2
Diameter of guide thimbles (lower part), mm	i.d 10.0 o.d 10.9	i.d 10.0 o.d 10.9
Diameter of instrument thimble, mm	i.d 11.4 o.d 12.2	i.d 11.4 o.d 12.2
Rod cluster control assemblies		
Neutron absorber full and part-length		
Composition	80%Ag-15%In-5%Cd	80%Ag-15%In-5%Cd
Density, g/cm^3	10	10.2
Diameter of absorber, mm	8.66	8.66
Cladding material	304SS	304SS
Clad outer diameter, mm	9.60	9.60
Clad thickness, mm	0.47	0.47
Number of clusters, full/part length	52/5	48/5
Number of absorber rods per cluster	24	24
Length of active section of part length absorber, mm	1047	914.4

CORE MECHANICAL DESIGN PARAMETERS	4267 mm Core (168 in)	3658-mm Core (12 ft)
Burnable poison rods (first core)		
Number	1040	1072
Material	Borosilicate glass	Borosilicate glass
Outside diameter, mm	9.68	9.68
Inner tube, o.d., mm	4.61	4.58
Clad material	stainless steel	stainless steel
Inner tube material	stainless steel	stainless steel
Boron loading (w/o B_2O_3 in glass rod)	12.5	12.5
Weight of B-10 per length of rod, kg/m	$0.623 \cdot 10^{-3}$	$0.623 \cdot 10^{-3}$
Core structure		
Material	304SS	304SS
Core barrel, i.d/o.d, mm	3400/3502	3400/3502
Thermal shield	Neutron pad design	Neutron pad design
i.d/o.d, mm	(4 pads bolted and pinned to the outside of the core barrel.) Dimensions at each pad: width 1220 mm, length 3744 mm, thickness 68 mm	3648/3759

NUCLEAR DESIGN PARAMETERS	4267-mm Core (168 in)	3658-mm Core (12 ft)
Structure characteristics		
Core diameter, mm (equivalent)	3040	3040
Core average active fuel height, mm	4267	3658
Reflector thickness and composition		
Top - water plus steel, mm	∿ 250	∿ 250
Bottom - water plus steel, mm	∿ 250	∿ 250
Side - water plus steel, mm	∿ 380	∿ 380
Fuel enrichment, w/o (see Fig.2)		
Region 1	2.10	2.10
Region 2	2.60	2.60
Region 3	3.10	3.10

APPENDIX B

The material number densities given below were used for calculating the nuclear cross sections for fuel assemblies and side reflectors, Cp. 3. The number densities correspond to an average fuel temperature of 675 °C, and an average cladding temperature of 350 °C.

The fuel pin cell

(see Fig. 10)

Cell region	Material	Number densities (10^{24} Atoms/cm^3)		
		Part of core (see Fig. 2)		
Fuel		Region 1	Region 2	Region 3
	U 235	$4.99 \cdot 10^{-4}$	$6.18 \cdot 10^{-4}$	$7.37 \cdot 10^{-4}$
	U 238	$2.30 \cdot 10^{-2}$	$2.29 \cdot 10^{-2}$	$2.28 \cdot 10^{-2}$
	O	$4.70 \cdot 10^{-2}$	$4.70 \cdot 10^{-2}$	$4.70 \cdot 10^{-2}$
Cladding				
	Fe		$7.59 \cdot 10^{-4}$	
	Ni		$1.69 \cdot 10^{-3}$	
	Cr		$7.30 \cdot 10^{-4}$	
	Zr		$3.77 \cdot 10^{-2}$	
	Al		$1.28 \cdot 10^{-3}$	
	C		$6.04 \cdot 10^{-6}$	
	Ti		$3.03 \cdot 10^{-5}$	

Moderator		Void percent				
		0 %	5 %	10 %	20 %	80 %
	H	$4.72 \cdot 10^{-2}$	$4.51 \cdot 10^{-2}$	$4.31 \cdot 10^{-2}$	$3.91 \cdot 10^{-2}$	$1.49 \cdot 10^{-2}$
	O	$2.36 \cdot 10^{-2}$	$2.26 \cdot 10^{-2}$	$2.16 \cdot 10^{-2}$	$1.95 \cdot 10^{-2}$	$7.44 \cdot 10^{-3}$
for 900 ppm B	B10	$6.89 \cdot 10^{-6}$	$6.59 \cdot 10^{-6}$	$6.30 \cdot 10^{-6}$	$5.71 \cdot 10^{-6}$	$2.18 \cdot 10^{-6}$
	B11	$2.84 \cdot 10^{-5}$	$2.72 \cdot 10^{-5}$	$2.60 \cdot 10^{-5}$	$2.36 \cdot 10^{-5}$	$8.98 \cdot 10^{-5}$

The water pin cell

(see Fig. 12)

Cell region	Material	Number densities (10^{24} Atoms/cm^3)
Inner moderator		As for the moderator region of the fuel pin cell, but 0% void assumed.
Guide thimble		
	Fe	$9.06 \cdot 10^{-4}$
	Ni	$2.04 \cdot 10^{-3}$
	Cr	$8.77 \cdot 10^{-4}$
	Zr	$4.22 \cdot 10^{-2}$
	Al	$1.44 \cdot 10^{-3}$
	C	$7.30 \cdot 10^{-6}$
	Ti	$3.66 \cdot 10^{-5}$
Outer moderator		As for the moderator region of the fuel pin cell.

The control pin cell

(see Fig. 13)

Cell region	Material	Number densities (10^{24} Atoms/cm^3)
Absorber		
	Ag	$4.49 \cdot 10^{-2}$
	In	$7.91 \cdot 10^{-3}$
	Cd_0	$2.01 \cdot 10^{-3}$
	Cd_i	$6.76 \cdot 10^{-4}$
Absorber cladding		
	Cr	$1.73 \cdot 10^{-2}$
	Ni	$8.08 \cdot 10^{-3}$
	Fe	$6.03 \cdot 10^{-2}$
Inner moderator		
Guide thimble		As for the water pin cell
Outer moderator		

The boron pin cell

(see Fig. 14)

Cell region	Material	Number densities (10^{24} Atoms/cm^3)
Absorber	B 10	$6.586 \cdot 10^{-4}$
	B 11	$2.634 \cdot 10^{-3}$
	O	$2.195 \cdot 10^{-3}$
Absorber cladding		Not represented
Inner moderator		
Guide thimble		As for the water pin cell
Outer moderator		

APPENDIX C

Nuclear cross sections for the fuel assemblies given in Table 1, p. 19, are listed below as functions of

Boron: The moderator boron concentration in ppm
Temperature: The fuel average temperature in K
Density: The moderator density in g/cm^3

The units are:

Diffusion constants: cm
Cross sections: cm^{-1}

Fuel Assembly no. 1

without Xe/Sm

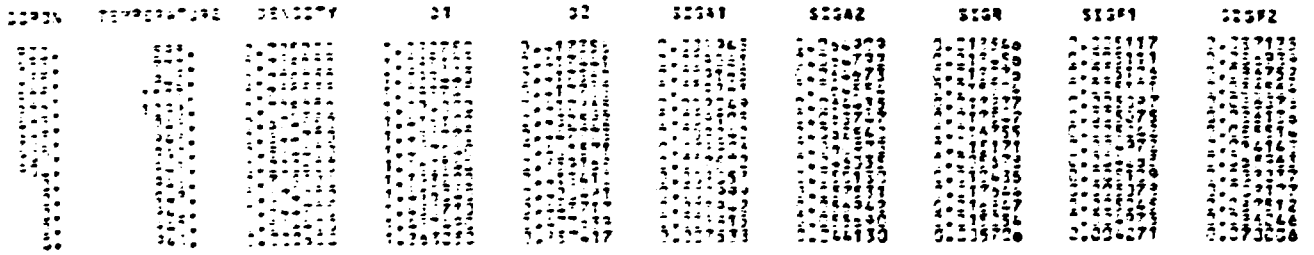

Xe/Sm in equilibrium concentration

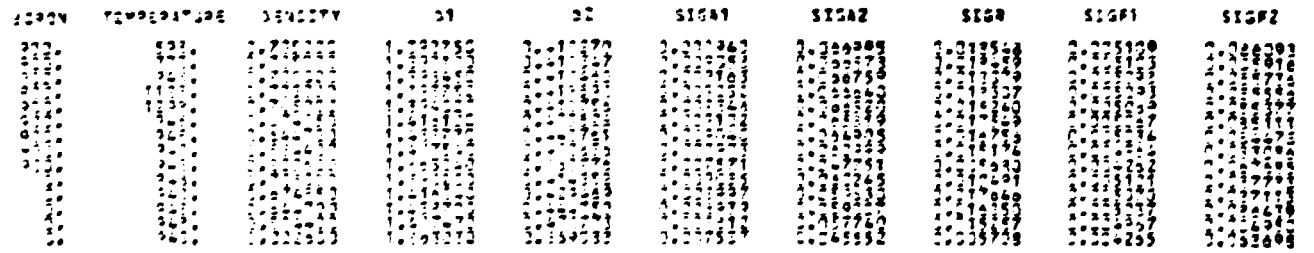

Fuel Assembly nc. 2

without Xe/Sm

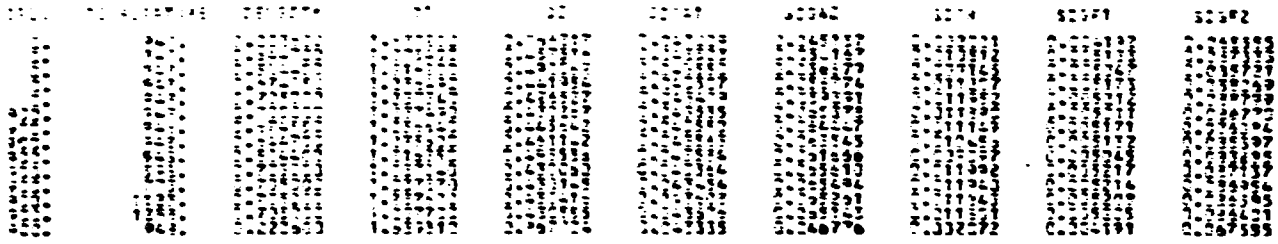

Xe/Sm in equilibrium concentration

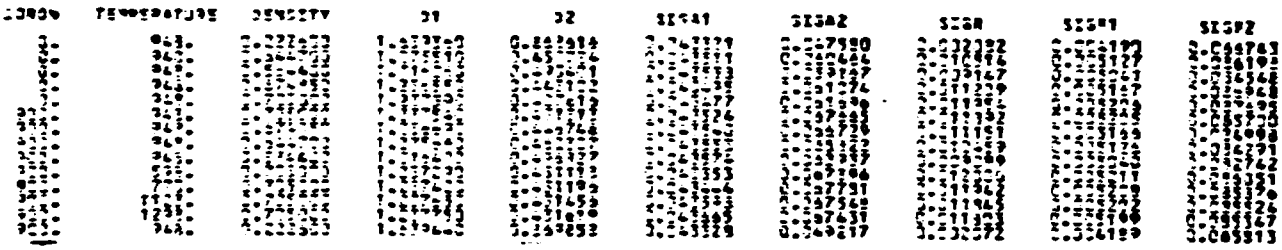

Fuel Assembly no. 3

Without Xe/Sm

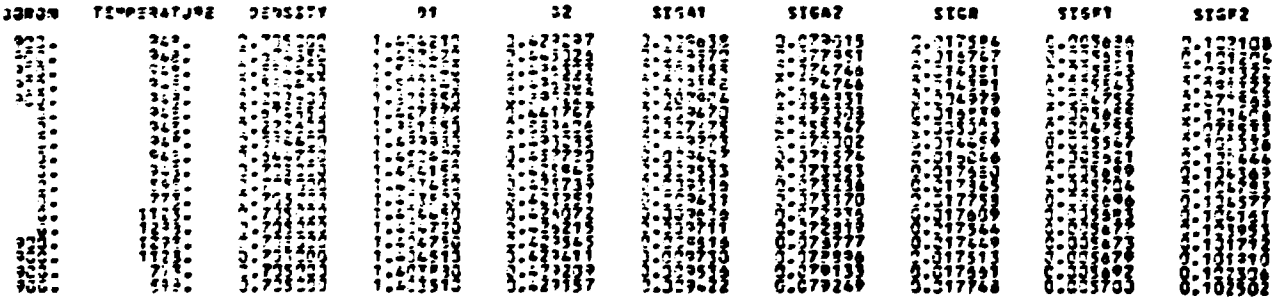

Xe/Sm in equilibrium concentration

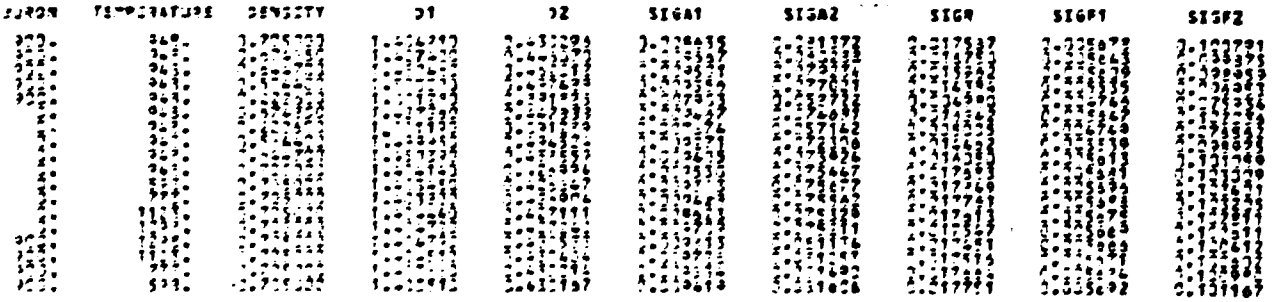

Fuel Assembly no. 4

Without Xe/Sm

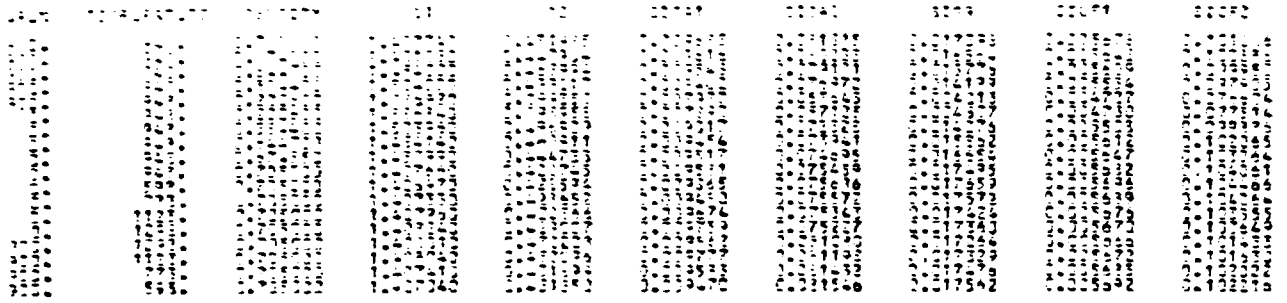

Xe/Sm in equilibrium concentration

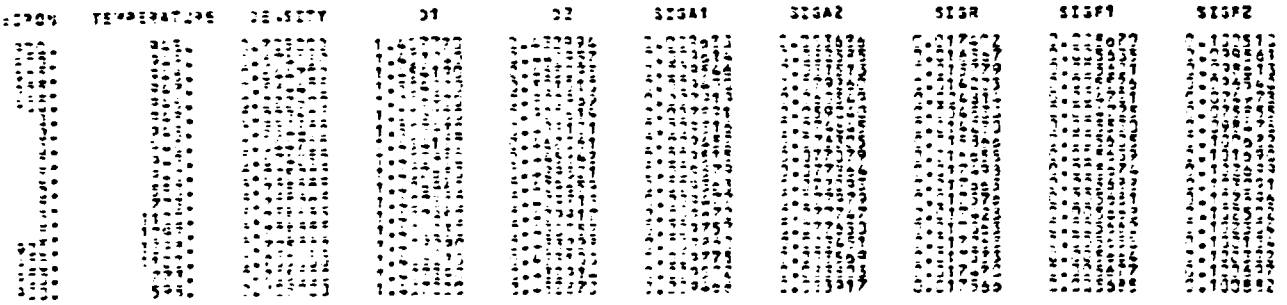

Fuel Assembly no. 5

Without Xe/Sm

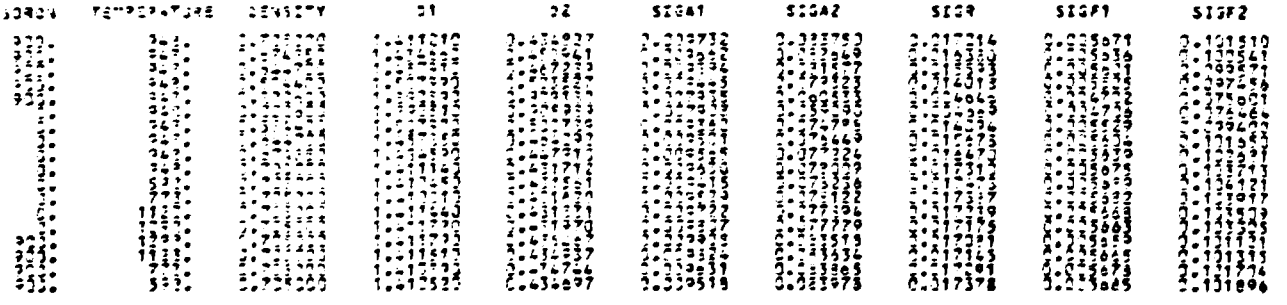

Xe/Sm in equilibrium concentration

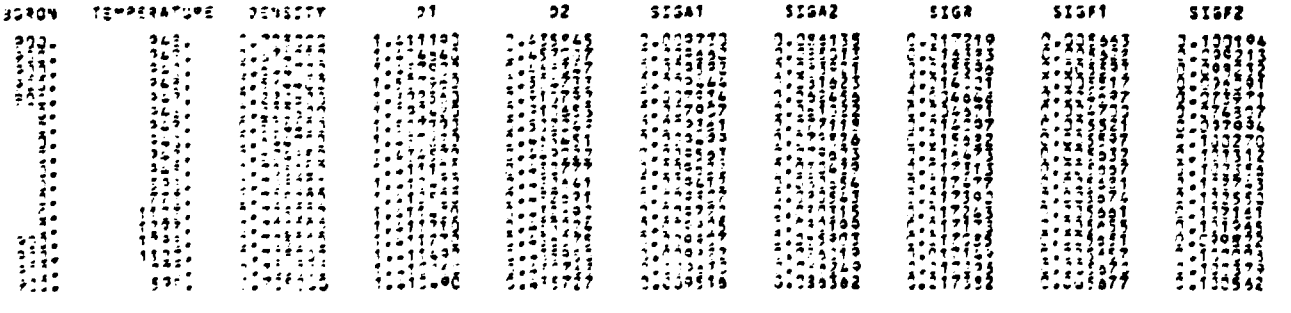

Fuel Assembly no. 6

Without Xe/Sm

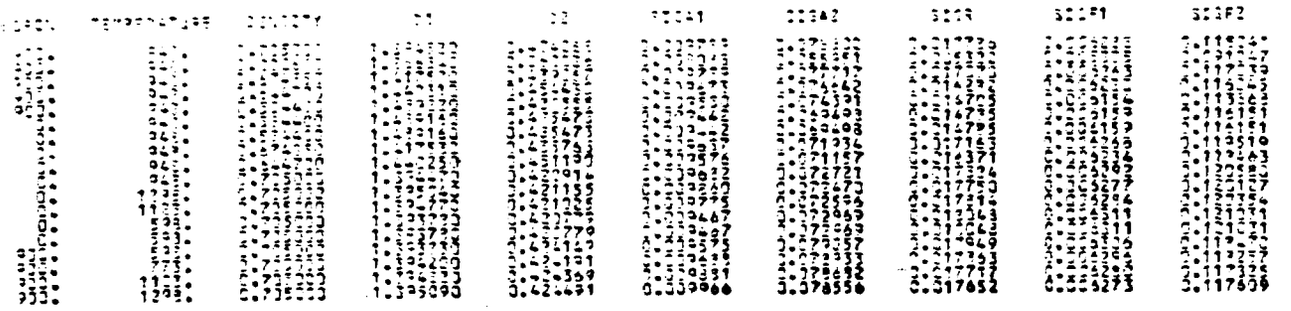

Xe/Sm in equilibrium concentration

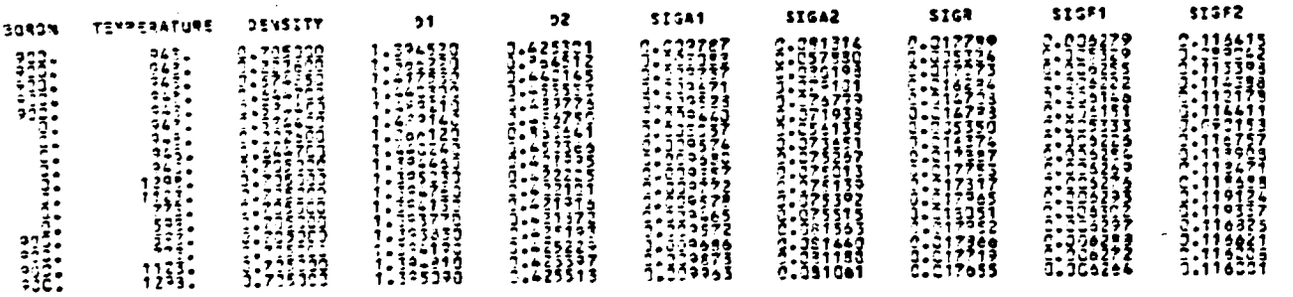

Fuel Assembly no. 7

Without Xe/Sm

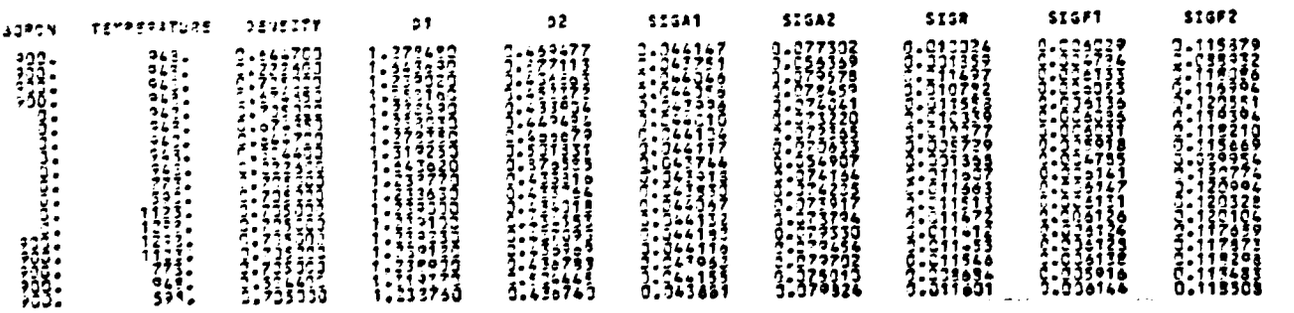

Xe/Sm in equilibrium concentration

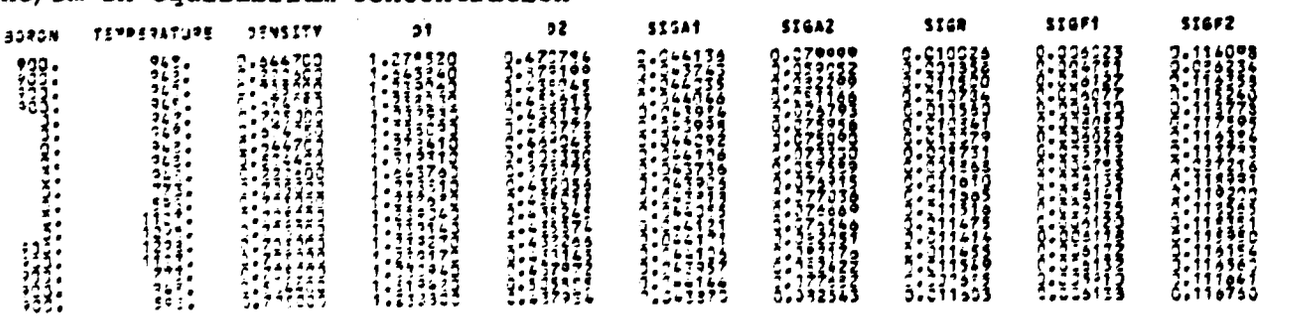

Fuel Assembly no. 8

Without Xe/Sm

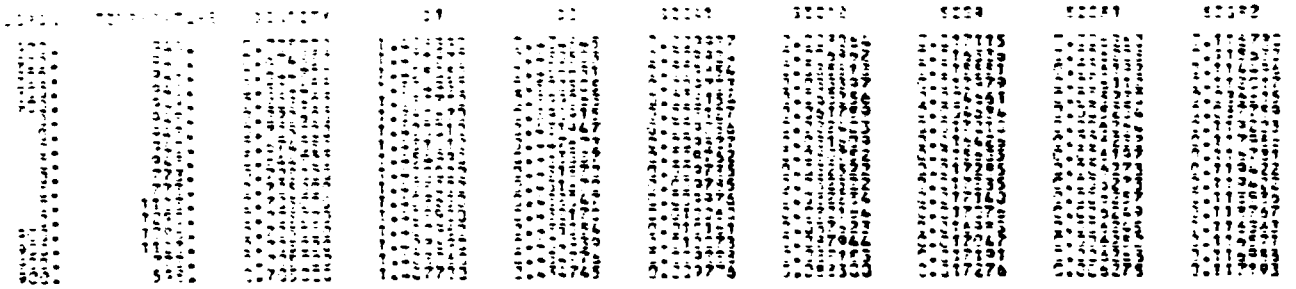

Xe/Sm in equilibrium concentration

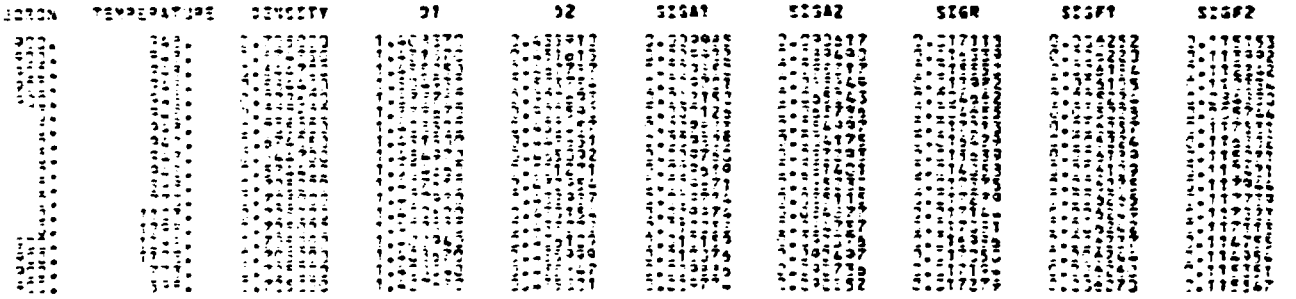

Fuel Assembly no.9

Without Xe/Sm

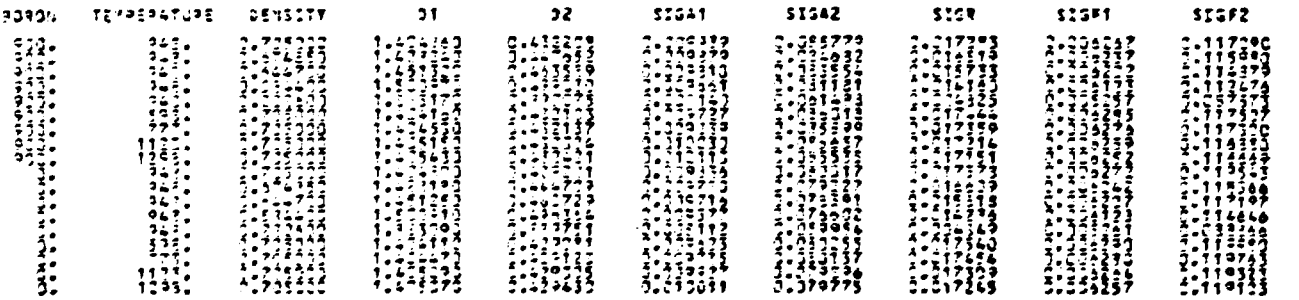

Xe/Sm in equilibrium concentration

APPENDIX D

Polynomial coefficients for the fuel assembly cross sections are listed below. The first 33 numbers in each group correspond to c_i, i = 1,33 given in Equation 4.3.2, p. 26. The remaining three numbers, representing ν_1, and the fission spectrum, respectively, refer to the reference condition and are needed for TWODIM calculations only.

The reference condition is

fuel temperature : 675 ^{o}C
moderator density : 705 kg/m^3
boron concentration: 900 ppm

Polynomial coefficients for assemblies 1-9.
New fuel without Xe and Sm.

```
1
.1393E+01-.5146E+00 .3814E+00 .4173E+00-.1121E+01 .8342E+00-.2912E+01
.4650E-05 .1838E-01 .1501E+01 .5562E+00 .9592E+00-.1449E-02-.6288E-05
.9162E-02 .1939E+00-.3330E+00 .3815E-02 .1168E-04 .6465E-01 .4294E+00
-.3481E+00 .7243E-05 .1475E+01 .5106E-02 .1770E+00-.3370E+00 .8673E-01
.1999E+00-.4370E+00-.2325E-05 .1019E+01 .2430E+01 .2589E+01 .1300E+01
.3732E-09
2
.1238E+01-.4811E+00 .3974E+00 .4300E+00-.1119E+01 .7978E+00-.2634E+01
.5780E-05 .1189E-01 .2072E+01 .1145E+01 .3272E+00-.1633E-02-.5698E-05
.4353E-01-.1553E-01-.3014E-01 .6181E-03 .9262E-06 .6536E-01 .4267E+00
-.3380E+00 .6621E-05 .1519E+01 .5210E-02 .2176E+00-.3890E+00 .9675E-01
.2143E+00-.5054E+00-.2260E-05 .1063E+01 .2430E+01 .2636E+01 .1000E+01
.3772E-09
3
.1404E+01-.5206E+00 .3805E+00 .4288E+00-.1175E+01 .6711E+00-.3187E+01
.5649E-05 .1758E-01 .1586E+01 .7732E+00 .1173E+01-.1672E-02-.6176E-05
.9632E-02 .1920E+00-.3619E+00 .3556E-02 .1117E-04 .7900E-01 .3983E+00
-.3308E+00 .6602E-05 .1530E+01 .5687E-02 .1671E+00-.3593E+00 .1021E+00
.2428E+00-.5291E+00-.2516E-05 .1180E+01 .2430E+01 .2574E+01 .1000E+01
.3732E-09
4
.1408E+01-.5225E+00 .3793E+00 .4316E+00-.1196E+01 .5173E+00-.3491E+01
.5370E-05 .1740E-01 .1592E+01 .6873E+00 .1028E+01-.1482E-02-.6120E-05
.9679E-02 .1938E+00-.3681E+00 .3523E-02 .1088E-04 .8129E-01 .3934E+00
-.3823E+00 .6479E-05 .1545E+01 .5680E-02 .1705E+00-.3660E+00 .1018E+00
.2555E+00-.5342E+00-.2499E-05 .1216E+01 .2430E+01 .2574E+01 .1000E+01
.3732E-09
5
.1611E+01-.5240E+00 .3794E+00 .4343E+00-.1203E+01 .5221E+00-.3530E+01
.5021E-05 .1721E-01 .1609E+01 .7013E+00 .1046E+01-.1491E-02-.6104E-05
.9726E-02 .1950E+00-.3763E+00 .3491E-02 .1069E-04 .8372E-01 .3885E+00
-.3856E+00 .6349E-05 .1562E+01 .5673E-02 .1722E+00-.3768E+00 .1015E+00
.2644E+00-.5440E+00-.2465E-05 .1249E+01 .2430E+01 .2575E+01 .1000E+01
.3732E-09
6
.1395E+01-.5183E+00 .3792E+00 .4242E+00-.1129E+01 .8080E+00-.2686E+01
.5284E-05 .1779E-01 .1336E+01-.1044E+01-.1664E+01-.1440E-02-.6122E-05
.9787E-02 .1614E+00-.4114E+00 .3485E-02 .1169E-04 .7880E-01 .4242E+00
-.3664E+00 .6742E-05 .1637E+01 .6292E-02 .1318E+00-.3802E+00 .1130E+00
.2392E+00-.4863E+00-.2858E-05 .7962E+00 .2430E+01 .2562E+01 .1000E+01
.3732E-09
7
.1239E+01-.4949E+00 .3774E+00 .4364E+00-.1198E+01 .4095E+00-.3036E+01
.5320E-05 .1150E-01 .2174E+01 .1259E+01 .7356E+00-.1420E-02-.5860E-05
.4404E-01-.3548E-01-.1001E+00 .5916E-03 .1074E-05 .7955E-01 .4285E+00
-.3649E+00 .6120E-05 .1536E+01 .6134E-02 .2447E+00-.4381E+00 .1181E+00
.2414E+00-.5182E+00-.2757E-05 .1202E+01 .2430E+01 .2608E+01 .1000E+01
.3732E-09
8
.1408E+01-.5252E+00 .3764E+00 .4343E+00-.1163E+01 .7919E+00-.2930E+01
.4589E-05 .1712E-01 .1510E+01-.1119E+00-.2370E+00-.1475E-02-.6086E-05
.9983E-02 .1877E+00-.3877E+00 .3337E-02 .1049E-04 .8805E-01 .3900E+00
-.4019E+00 .6291E-05 .1540E+01 .6262E-02 .1522E+00-.3914E+00 .1168E+00
.2798E+00-.5220E+00-.2653E-05 .1261E+01 .2430E+01 .2562E+01 .1000E+01
.3732E-09
9
.1405E+01-.5229E+00 .3788E+00 .4317E+00-.1158E+01 .7171E+00-.3033E+01
.4936E-05 .1738E-01 .1467E+01-.3439E+00-.5927E+00-.1467E-02-.6080E-05
.9934E-02 .1787E+00-.3949E+00 .3384E-02 .1057E-04 .8576E-01 .3915E+00
-.4054E+00 .6374E-05 .1530E+01 .6270E-02 .1456E+00-.3909E+00 .1171E+00
.2644E+00-.5233E+00-.2744E-05 .1222E+01 .2430E+01 .2562E+01 .1000E+01
.3732E-09
```

Polynomial coefficients for assemblies 1-9. New fuel, but with Xe and Sm in equilibrium concentrations.

```
1
 .1394E+01-.5145E+00 .3814E+00 .4182E+00-.1124E+01 .8355E+00-.2899E+01
 .6545E-05 .1838E-01 .1501E+01 .5581E+00 .8625E+00-.1450E-02-.6294E-05
 .9159E-02 .1937E+00-.3324E+00 .3817E-02 .1170E-04 .6674E-01 .4220E+00
-.3485E+00 .7211E-05 .1474E+01 .5099E-02 .1772E+00-.3360E+00 .8571E-01
 .1956E+00-.4989E+00-.2282E-05 .1029E+01 .2430E+01 .2539E+01 .1000E+01
 .3732E-09
2
 .1238E+01-.4811E+00 .3975E+00 .4311E+00-.1121E+01 .8019E+00-.2621E+01
 .5612E-05 .1189E-01 .2072E+01 .1151E+01 .8386E+00-.1433E-02-.5722E-05
 .4352E-01-.1569E-01-.5007E-01 .6137E-03 .9539E-06 .6764E-01 .4158E+00
-.3096E+00 .6597E-05 .1511E+01 .5204E-02 .2171E+00-.3879E+00 .8568E-01
 .2208E+00-.5389E+00-.2223E-05 .1086E+01 .2430E+01 .2637E+01 .1000E+01
 .3732E-09
3
 .1404E+01-.5211E+00 .3794E+00 .4298E+00-.1190E+01 .5152E+00-.3438E+01
 .5573E-05 .1759E-01 .1577E+01 .6871E+00 .1034E+01-.1473E-02-.6099E-05
 .9630E-02 .1923E+00-.3606E+00 .3558E-02 .1111E-04 .8135E-01 .3946E+00
-.3779E+00 .6555E-05 .1529E+01 .5679E-02 .1688E+00-.3554E+00 .1008E+00
 .2516E+00-.5378E+00-.2481E-05 .1194E+01 .2430E+01 .2575E+01 .1000E+01
 .3732E-09
4
 .1408E+01-.5225E+00 .3795E+00 .4325E+00-.1196E+01 .5199E+00-.3472E+01
 .5258E-05 .1740E-01 .1593E+01 .6955E+00 .1042E+01-.1482E-02-.6098E-05
 .9677E-02 .1935E+00-.3685E+00 .3525E-02 .1091E-04 .8366E-01 .3894E+00
-.3806E+00 .6439E-05 .1545E+01 .5672E-02 .1704E+00-.3658E+00 .1005E+00
 .2623E+00-.5475E+00-.2449E-05 .1226E+01 .2430E+01 .2575E+01 .1000E+01
 .3732E-09
5
 .1411E+01-.5239E+00 .3795E+00 .4353E+00-.1203E+01 .5243E+00-.3512E+01
 .4910E-05 .1722E-01 .1609E+01 .7050E+00 .1052E+01-.1492E-02-.6079E-05
 .9725E-02 .1948E+00-.3764E+00 .3493E-02 .1072E-04 .8611E-01 .3849E+00
-.3832E+00 .6309E-05 .1562E+01 .5665E-02 .1721E+00-.3764E+00 .1002E+00
 .2733E+00-.5576E+00-.2418E-05 .1260E+01 .2430E+01 .2575E+01 .1000E+01
 .3732E-09
6
 .1395E+01-.5186E+00 .3783E+00 .4248E+00-.1142E+01 .6340E+00-.3035E+01
 .5768E-05 .1779E-01 .1346E+01-.9387E+00-.1487E+01-.1442E-02-.5960E-05
 .9783E-02 .1650E+00-.3913E+00 .3478E-02 .1116E-04 .8129E-01 .4110E+00
-.3862E+00 .6688E-05 .1482E+01 .6282E-02 .1316E+00-.3780E+00 .1164E+00
 .2405E+00-.5115E+00-.2801E-05 .1140E+01 .2430E+01 .2562E+01 .1000E+01
 .3732E-09
7
 .1239E+01-.4949E+00 .3776E+00 .4376E+00-.1199E+01 .4134E+00-.3016E+01
 .4976E-05 .1150E-01 .2174E+01 .1260E+01 .7372E+00-.1420E-02-.5865E-05
 .4403E-01-.3555E-01-.9991E-01 .5919E-03 .1097E-05 .8227E-01 .4202E+00
-.3427E+00 .6085E-05 .1533E+01 .6128E-02 .2442E+00-.4376E+00 .1163E+00
 .2708E+00-.5506E+00-.2707E-05 .1220E+01 .2430E+01 .2608E+01 .1000E+01
 .3732E-09
8
 .1408E+01-.5241E+00 .3790E+00 .4354E+00-.1168E+01 .7043E+00-.3079E+01
 .4585E-05 .1712E-01 .1511E+01-.9377E-01-.2060E+00-.1477E-02-.6143E-05
 .9980E-02 .1828E+00-.3973E+00 .3355E-02 .1036E-04 .9060E-01 .3826E+00
-.4103E+00 .6214E-05 .1545E+01 .6254E-02 .1500E+00-.3960E+00 .1151E+00
 .2825E+00-.5454E+00-.2659E-05 .1266E+01 .2430E+01 .2562E+01 .1000E+01
 .3732E-09
9
 .1405E+01-.5227E+00 .3789E+00 .4328E+00-.1159E+01 .7192E+00-.3015E+01
 .4885E-05 .1729E-01 .1465E+01-.3485E+00-.5982E+00-.1468E-02-.6130E-05
 .9931E-02 .1781E+00-.3956E+00 .3386E-02 .1055E-04 .8830E-01 .3884E+00
-.4046E+00 .6329E-05 .1529E+01 .6262E-02 .1452E+00-.3911E+00 .1154E+00
 .2720E+00-.5367E+00-.2691E-05 .1234E+01 .2430E+01 .2562E+01 .1000E+01
 .3732E-09
```

APPENDIX E

Normalized horizontal power distributions for Beaver Valley unit 1. TWODIM calculations referred to Westinghouse results.

Relative assembly powers for one octant of an unrodded core near beginning of life is shown below. The reactor state is hot full power with 916 ppm boron in the coolant. For the sub-reflector inside the core baffle cross-sectional representation is used, while the remaining reflector is represented by gamma-matrices.

Key:
Upper value: Westinghouse
Lower value: TWODIM

No Xenon

1.14	1.08	1.19	1.10	1.21	1.19	1.06	0.82
1.16	1.14	1.20	1.14	1.18	1.18	1.02	0.85
	1.18	1.17	1.20	1.14	1.14	1.01	0.62
	1.20	1.21	1.19	1.15	1.10	1.00	0.68
		1.21	1.14	1.12	0.98	0.90	
		1.21	1.15	1.08	0.96	0.90	
			1.11	0.97	0.90	0.59	
			1.08	0.95	0.87	0.60	
				0.84	0.62		
				0.79	0.65		

Equilibrium Xenon

1.16	1.09	1.21	1.11	1.21	1.18	1.05	0.80
1.18	1.15	1.21	1.15	1.18	1.18	1.01	0.82
	1.20	1.18	1.21	1.14	1.14	0.99	0.61
	1.21	1.22	1.20	1.15	1.10	0.99	0.66
		1.22	1.14	1.13	0.98	0.88	
		1.21	1.16	1.09	0.96	0.89	
			1.12	0.97	0.89	0.59	
			1.08	0.95	0.87	0.60	
				0.85	0.62		
				0.79	0.65		

APPENDIX F

Comparison of normalized horizontal power distributions calculated with ANTI and TWODIM for different core configurations.

The values represent the relative channel power from ANTI minus the corresponding channel power from TWODIM. One octant of the core, representing channels no. 1-26, is shown. The power shape is altered either by inserting control assemblies or by increasing the fission cross sections locally.

For the tables below, the key is

Upper value: Channel no.
Lower value: Power deviation as defined above.

ANTI representation: One node per cross section of channel. (Coupling coefficients as in Eq. 5.2.11).

Unrodded standard core:

1	2	3	4	5	6	7	8
0.07	0.03	0.05	-0.02	-0.02	-0.05	-0.07	-0.05
	9	10	11	12	13	14	15
	0.06	0.02	0.01	-0.03	-0.04	-0.01	-0.02
		16	17	18	19	20	
		0.03	0.00	-0.02	-0.05	0.02	
			21	22	23	24	
			0.01	-0.03	0.10	0.03	
				25	26		
				-0.03	0.02		

Control in channel no 1:

1	2	3	4	5	6	7	8
-0.03	0.09	0.06	0.00	-0.02	-0.06	-0.09	-0.07
	9	10	11	12	13	14	15
	0.12	0.06	0.02	-0.03	-0.05	-0.02	-0.04
		16	17	18	19	20	
		0.05	0.00	-0.03	-0.006	0.01	
			21	22	23	24	
			0.01	-0.03	0.11	0.03	
				25	26		
				-0.04	0.01		

Control in channel no. 23:

1	2	3	4	5	6	7	8
0.00	-0.04	-0.01	-0.04	-0.03	-0.06	-0.07	-0.06
	9	10	11	12	13	14	15
	0.00	-0.03	-0.01	-0.02	-0.04	0.00	-0.02
		16	17	18	19	20	
		0.00	-0.01	0.05	0.02	0.09	
			21	22	23	24	
			0.02	0.04	-0.04	0.05	
				25	26		
				0.07	0.02		

Control in channel no. 24:

1	2	3	4	5	6	7	8
0.00	-0.03	-0.01	-0.04	-0.03	-0.05	-0.08	-0.05
	9	10	11	12	13	14	15
	0.00	-0.03	-0.02	-0.03	-0.02	-0.01	0.02
		16	17	18	19	20	
		-0.01	-0.02	-0.01	0.02	0.07	
			21	22	23	24	
			0.01	0.00	0.16	-0.01	
				25	26		
				0.02	0.07		

Fission cross sections increased by 10% for channel no. 6:

1	2	3	4	5	6	7	8
0.07	0.04	0.05	0.00	-0.02	0.01	-0.08	-0.06
	9	10	11	12	13	14	15
	0.07	0.04	0.01	-0.04	-0.04	-0.02	-0.04
		16	17	18	19	20	
		0.03	0.00	-0.02	-0.05	0.02	
			21	22	23	24	
			0.01	-0.02	0.09	0.03	
				25	26		
				-0.02	0.02		

ANTI representation: Four nodes per cross section of channel. (Coupling coefficients as in Eq. 5.2.12)

Unrodded standard core:

1	2	3	4	5	6	7	8
0.02	0.08	0.01	0.03	-0.07	-0.06	-0.09	0.01
	9	10	11	12	13	14	15
	0.00	0.04	-0.04	-0.02	-0.09	0.02	0.06
		16	17	18	19	20	
		-0.04	0.01	-0.07	-0.01	0.05	
			21	22	23	24	
			-0.05	0.00	0.01	0.06	
				25	26		
				-0.03	0.07		

Control in channel no. 1:

1	2	3	4	5	6	7	8
0.08	0.06	-0.02	0.03	-0.08	-0.07	-0.10	0.02
9	10	11	12	13	14	15	
0.01	0.03	-0.05	-0.02	-0.09	0.02	0.07	
16	17	18	19	20			
-0.04	0.00	-0.07	-0.01	0.05			
21	22	23	24				
-0.05	0.01	0.01	0.09				
25	26						
-0.04	0.08						

Control in channel no. 23:

1	2	3	4	5	6	7	8
0.01	0.10	-0.04	0.04	-0.09	-0.07	-0.11	-0.05
9	10	11	12	13	14	15	
-0.02	0.04	-0.06	-0.01	-0.09	0.01	0.06	
16	17	18	19	20			
-0.06	0.01	-0.04	0.01	0.05			
21	22	23	24				
-0.04	0.02	0.06	0.04				
25	26						
0.01	0.03						

Control in channel no. 24:

1	2	3	4	5	6	7	8
0.03	0.10	-0.02	0.05	-0.08	-0.06	-0.10	0.01
9	10	11	12	13	14	15	
0.00	0.04	-0.05	-0.01	-0.07	0.01	0.06	
16	17	18	19	20			
-0.04	0.01	-0.06	0.01	0.03			
21	22	23	24				
-0.04	0.02	0.02	0.04				
25	26						
-0.01	0.07						

Fission cross sections increased by 10% for channel no. 6:

1	2	3	4	5	6	7	8
0.08	0.03	0.04	0.04	-0.12	-0.19	-0.18	-0.03
	9	10	11	12	13	14	15
	0.05	0.08	-0.02	-0.03	-0.15	-0.05	0.04
		16	17	18	19	20	
		0.01	0.04	-0.05	-0.02	0.04	
			21	22	23	24	
			-0.02	0.03	0.02	0.09	
				25	26		
				-0.01	0.09		

Risø National Laboratory **Risø - M - 2264**

Risø - M - 2264

Title and author(s)

CONSTRUCTION OF PWR NUCLEAR CROSS SECTIONS FOR TRANSIENT CALCULATIONS. TEST OF THE ANTI PROGRAM AGAINST TWODIM

Bjørn Thorlaksen

Date 1981-06-02

Department or group

Department of Reactor Technology

Group's own registration number(s)

57 pages + tables + illustrations

Abstract

Nuclear cross sections for fuel assemblies of the more recent Westinghouse designs, representing two different PWR reactor cores, are calculated as functions of average fuel temperature, moderator density, and moderator poison concentration. The cross-sections are verified by referring to Westinghouse power-shape calculations and other analysis.

Computations on the side reflector resulted in significantly higher albedo values than used previously for BWR's in similar nodal codes. This led to an investigation of the influence of the internodal coupling coefficients on the power shape. It is concluded that the calculated power shape is strongly dependent, on the choice of coupling coefficients. However, it is shown that "the correct" set of coupling coefficients depends mostly on the nodal configuration, and that it is fairly independent of the power condition.

Copies to

Library 100

Department of Reactor Technology 25

Available on request from Risø Library, Risø National Laboratory (Risø Bibliotek), Forsøgsanlæg Risø), DK-4000 Roskilde, Denmark
Telephone: (03) 37 12 12, ext. 2262. Telex: 43116